AN INTELLIGENT SYSTEM FOR TEMPERATURE MONITORING AND BRAKE DRUM COOLING

By

Rahul Sable

A Dissertation Submitted in

Partial Fulfillment of the Requirements for the

Master of Science in Mechanical Engineering

Faculty of Mechanical Engineering

Lakehead University

August 2018

Abstract

Brakes convert the kinetic energy of the moving vehicle into heat energy due to friction between fixed and moving brake parts. Frequent applications of the brakes will cause overheating in brake parts, which could generate the lubricating layer between frictional parts and result in a temporary reduction or complete loss of braking power of a vehicle. Several brake cooling methods have been proposed in the literature to solve this problem, but the effective brake cooling is still a challenging task in trucks. The objective of this research is to develop an intelligent system for temperature monitoring and active cooling in drum brakes for heavy utility trucks. The air is used as the medium of the cooling system. The buildup heat is dissipated by use of air blow across the brake elements. The cooling system incorporates an automatic controller. A specifically designed air compressor is used to discharge air with a high flow rate. Temperature is measured by using an infra-red thermal sensor. The air cooling is turned ON when the brake drum temperature is higher than a threshold value and is switched OFF once the temperature is lower than another threshold. This self-regulating controller and efficient air compressor play an integral role in the cooling system.

The second research project is to develop a piezoelectric energy harvesting system to provide power for infra-red temperature monitoring sensors. A new energy harvesting model is proposed to generate power from the ambient vibration of the vehicle. A moving vehicle generates vibrations with different frequencies. A general piezoelectric system is efficient mainly around its resonance frequency. By systematic experimental tests, a new energy harvesting system is proposed to improve power generating capacity over a wider vibrational frequency range. The energy harvesting circuit stores power using piezoelectric transducer into battery, which in turn to charge temperature sensors. The effectiveness of the proposed energy harvesting methodology and system is verified experimentally under different excited frequencies.

Acknowledgments

Table of Contents

List of Figures

List of Tables

Chapter 1 Introduction

1.1 Vehicle Braking

A vehicle is an assembly of many systems incorporated together to perform controlled motions, which include a steering system, a driving unit (e.g., an engine or induction motor), a braking system, etc. It has no doubt that the brake system is critical to the vehicle operation and driving safety, which can respond to the driver's actions to reduce the speed of the vehicle or bring it to a stop. According to function principles, brake systems can be categorized as electrical, hydraulic, and frictional brakes [1]. The electric brakes are actuator devices which use electric current or magnetic force to slow down or stop motion of rotating wheels. Electric brakes are typically used in the hybrid car, trains, and trams. A hydraulic braking system transmits brake-pedal force to wheel brakes through the pressurized fluid; the fluid pressure converts to braking forces at the wheels [2]. On the other side, frictional brakes use frictional force to stop or slow down the vehicle from moving [3]. The frictional brakes are most commonly used in passenger vehicle and transportation trucks due to their light-weight as compared to the hydraulic braking system, low costs and easy to maintain; this work will focus on the analysis of frictional brakes.

Based on structures, frictional brakes are categorized as disc brakes and drum brakes as illustrated in Figure 1.1. The core parts of a disc brake are the brake pad and the brake disc rotor as shown in Figure 1.1(a). When an axial force is applied to brake pads against the rotor disc, the brake pads squeeze the disc rotor and generate the frictional force between disc brake components [4]. The brake frictional force is then transmitted to the wheel to stop or slow down the rotation of the wheel. Disc brakes are commonly used in passenger cars due to their light weight and better heat dissipation at moderate brake performance.
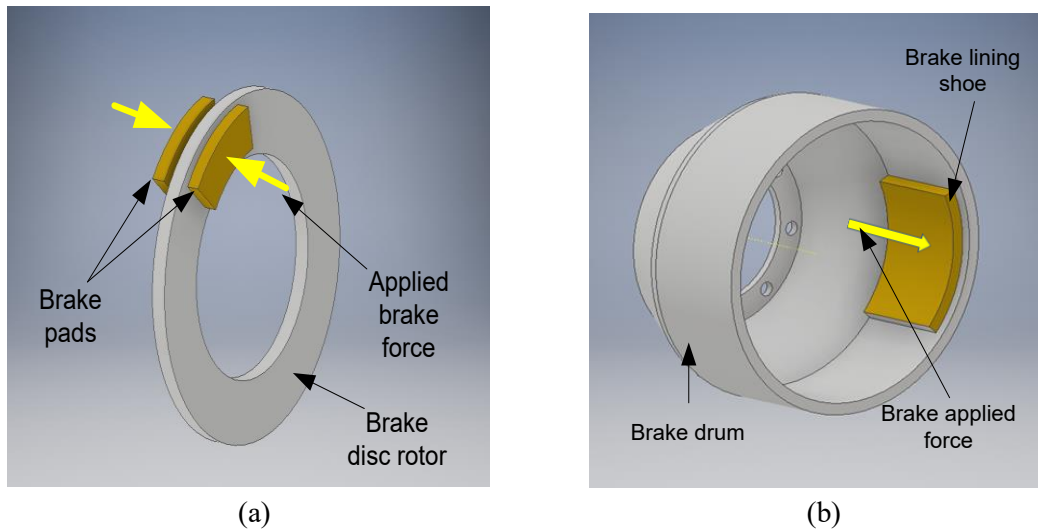
Figure 1.1. Schematic diagrams of (a) A disc brake, (b) A drum brake.

A drum brake mainly consists of a brake drum and a brake lining shoe as illustrated in Figure 1.1(b). The cylinder-shaped brake drum rotates with the wheel axle of the vehicle. The brake force is applied to push the brake lining shoe outwards to oppose the rotation of the brake drum. A drum brake has more frictional area than a disc brake, which can provide high braking forces [5]. Consequently, drum brakes are commonly used in heavy utility vehicles such as transportation trucks due to their higher braking power [6]. This thesis focuses on the analysis of drum brakes in transportation trucks.

1.2 Overheating of Drum Brakes

During operation, a brake transfers kinetic energy into thermal energy due to opposing frictional forces in order to control motion speed. The amount of generated heat is dependent on vehicle mass, rate of speed reduction, and braking operation frequency. When a truck is descending mountains or driving downhill, the brakes will be in operation continuously. More frictional heat is generated, and the temperature of drum brakes will increase steadily. For instance, some

simulation indicated that the temperature rate could reach up to 142°C over 1 second of brake engagement [7] and overheating problems can occur in truck brakes [8]. If the temperature of a drum brake is above some critical level, counter reactions could occur on the drum brake components; the micro-properties of brake component materials and brake structures may change, which will degrade braking operation and result in the following negative consequences.

1) Diminished Brake Performance

Braking heat is generated in the brake drum and the brake lining shoe. The brake lining shoe is composed of several soft base materials, embedded with tough asbestos particles using some bonding agents [9]. The bonding elements of the brake pad absorb heat from the hot brakes, which makes the surface layer qualitatively change from the solid state to mixed state of gases, liquid and solid. The friction modality of brake surface changes from dry friction to a combined state with gases and liquids [10], which will lead to decrease in frictional coefficient of the materials. The gradual formation of a lubricating layer between the brake drum and the lining shoe will make the brake pedal feel spongy in braking operation. Such a scale-down of a vehicle's braking power could generate significant safety issues such as tire overheating or even firing, as shown in Figure 1.2(a). If a truck moves downhill, the loss of stopping power could generate serious safety consequences for the driver and the vehicle. This brake overheating problem can also be observed in the transportation trucks on highway roads as represented in Figure 1.2(b), due to heavy load, high speed, and intermediate brake applications.

| (a) | (b) |
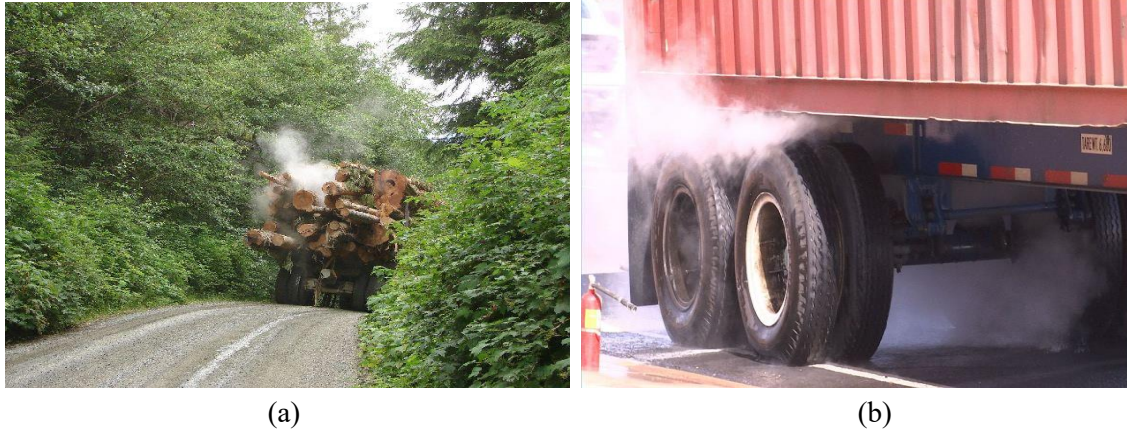
Figure 1.2. Overheated brake caught fire: (a) During downhill drive, (b) During high-way transportation (images retrieved from [11]).

2) Brake Component Thermal Wear

The high temperature in a brake system can also cause thermal wear problems, as shown in Figure 1.3. The overheating of the brake's lining shoe will cause some chemical reactions, resulting in the loss of mechanical strength. In addition, the high temperature can generate thermal stresses on the brake drum [12]. The thermal stress and loss of mechanical strength will cause a gradual increment in thermal wear that is generally governed by surface pitting, scoring, and severe wear [13]. The thermal wear effect will lead to early failure of the brake components, which is more predominant in heavy-duty vehicles such as transportation trucks.
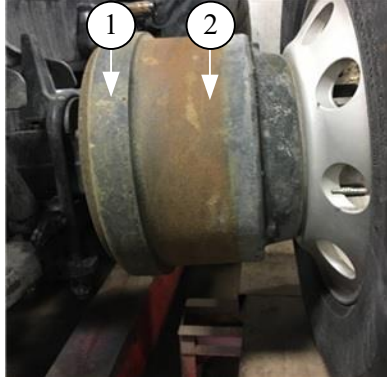
Figure 1.3. Thermal wear effect on the brake drum: (1) Brake drum, (2) Thermal wear effect.

The objective of this work is to develop an intelligent cooling system to monitor the brake temperature and cool the brakes, so as to improve braking efficiency and driving safety. A energy harvesting system will be developed to provide battery energy to cooling system.

Chapter 2 Literature Review and Research Objectives

2.1 Literature Review

In order to avoid brake drum's overheating problems as stated in Chapter 1; heat should be dissipated efficiently from brake components. Although heat can be transferred by natural convection, considering the high temperature involved in a brake system, a faster heat dissipation technique is necessary.

In general, the truck driver manually shifts the control to a lower gear transmission while going down a steep hill. This lower gear transmission can help slow down the speed of the vehicle without frequent use of brakes [14]. Considering this aspect, some technique was proposed to shift the gear automatically [15]. This technique includes a control system module that contains a temperature sensor, tilt sensor, and transmission shift positioning unit connected electrically. Specifically, the temperature sensor on brake measures the brake drum temperature, and tilt sensor estimates whether the vehicle is going up or down on the hill; based on the processed information, transmission positioning unit manipulates gear automatically in the transmission system. During downhill condition, if brake drum temperature is too high, system can alert driver regarding overheating of brakes. If the tilt sensor indicates a downhill inclination with brake overheating, the transmission position will be shifted to the lowest gear automatically. This system, however, could not provide an adequate cooling system for decrease temperature of the brake drum.

In order to avoid a brake drum's overheating problem, heat dissipation from brake components is an essential requirement. Generally, heat transfer achieved by using natural convection, but considering the high temperature involved, a faster heat dissipation technique is necessary. In general, a runaway truck ramp is a ramp with an up-surging slope to decrease the

speed of the vehicle until it reaches a resting point at the end of the ram [16]. The location of this constructed ramps is mostly in mountains areas. However, the number of built-up ramps is insufficient, and they are located only at specific locations. Therefore, the likelihood of collision due to overheating of brakes is higher if brake failure occurs in areas other than at the ramp locations.

Some of the active cooling strategies and systems are discussed as following.

1) Improved Brake Structure and Component Material

In recent years, Ashok Leyland Truck Ltd. introduced a concept of bimetal brake drum in order to increase heat transfer dissipation rate in drum brakes. Two types of brake drums were designed: the first one incorporated a cast-iron inner with an aluminum outer shell and clamping face. The second one used a cast-iron inner surface and clamping face, with an aluminum outer shell, as illustrated in Figure 2.1 These newly designed brake drums could increase heat dissipation by 33%, under testing conditions of 60 km/h with brake force applied for 1000 stops [17]. However, that new brake system cannot effectively overcome overheating problems.
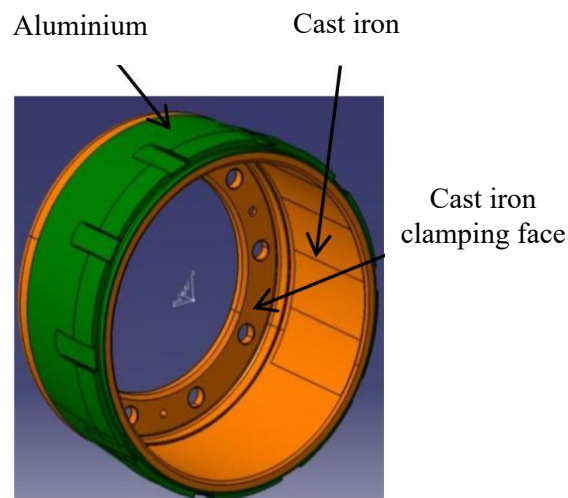
Figure 2.1. Bimetal brake drum (retrieved from [17]).

2) Water Cooling System

Researchers in [18] addressed the problem of functioning braking power under some critical temperature conditions. A new strategy was proposed to provide water spray inside the brake to cool the brake drum. The water spray setup enables draining water to cover the entire surface of the rim. One suction pipe is installed in the bottom portion of the brake to remove the remaining water from the brake system. This system, however, could operate only if the vehicle is in a stationary condition; the water spray and suction operations are controlled manually by hand levers in the vehicle driver compartment.

The brake overheating can be reduced by providing proper water supply to the brake drum. Bloss et al. investigated a solution to avoid direct contact between the cooling water and the brake drum; the cooling system consisted of a peripheral circular chamber around each brake drum [19]. The chamber has an inlet for water coolant and an outlet to discharge the water into the storage reservoir. A hand lever controls water flow through all chambers. The water in the storage reservoir tank is cooled naturally. The limitation imposed by such a system is related to its difficulties of mounting the chambers on the brake drum and its low efficiency in cooling.

In recent years, we have also witnessed some other types of brake drum cooling methods using water as a cooling medium. A water-spraying system was designed in [20], its cooling operation can be controlled either manually or automatically using a solenoid. In a manually controlled system a lever is used to adjust the flow of water. In the automatic controlling unit, a relay is used to control brake switch output as high or low. The vehicle operator's force on brake pedal triggers brake switch. If time duration of applied force to the brake pedal is longer than a threshold, the brake switch output becomes high, which generates higher flow rate of water on the

8

outer surface of the brake drum. Although water cooling has higher heat dissipation capacity, the use of water in frictional brakes can have some side-effects. For example, if water comes in contact with friction surfaces of brake drum and the brake lining shoe, water will act as a lubricant to reduce frictional force between brake components, which could lead to degraded braking efforts or even dangerous accident.

On the other hand, water cooling method is commonly used for racing trucks [21]. During truck racing, all four wheels tend to get overheated, which can hamper braking performance. In most Tata Prima racing trucks, temperature sensors are mounted on each of brake drum. If the temperature value is higher than a threshold, the controller actuates water flow to brake drum through nozzle jets from pressurized tanks. However, such a cooling system is controlled manually, and the water keeps spraying after the driver presses the brake pedal.

3) Air Cooling System

Another cooling method is based on air ventilation. The patent in [22] developed an air brake cooling system that operated with two cooling air reservoirs. The cooling air is supplied to the brake drum through an air pipe channel. The airflow is manually controlled by using a lever. Compressed air is first stored in a supplementary reservoir; the air is then cooled and filtered to clean foreign particles from brake drum before it is forced to the primary reservoir for cooling operations. The main limitation of this cooling method is related to its complexity because of the use of two air reservoirs and the related auxiliary systems.

Some other approaches have explored to solve the brake overheating problems by improving vehicle aerodynamics [23]. When the vehicle is in motion, some inlet ports are mounted on the front bumper of the vehicle to access of the air. The inlet port scoops transport the air to the

concave surface chamber to squeeze air over the concave surface and speed up the air flow rate. This air is forced to the outer surface of the brake drum for cooling. There has been some recent development observed in aerodynamic design to improve air moving in [24]. When the vehicle is in motion, the air is input to the duct on the vehicle bumper and flows forward to the brake drum through specific lead channels. However, it could be difficult to implement this technique for brake cooling in transportation trucks due to its relatively low speed of the truck and complex air transportation systems.

Another technique for drum brake cooling is to install an impeller rotor [25]. As illustrated in Figure 2.2, the impeller rotates and alters the flow of the gas or some liquid. The impeller contains some vanes. When the impeller rotates, a suction force is created to inhale air inside hollow compartment between the brake drum and the cover. However, the cooling efficiency using this technique depends on vehicle speed. If the vehicle speed is slow, the exerted air will have low flow rate, which may not be enough to cool the brake drums.
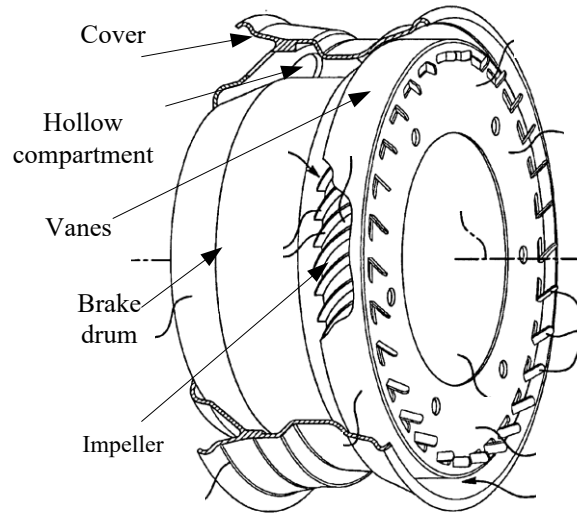
Figure 2.2. Brake drum cooling apparatus with impeller setup (image retrieved from [25]).

Another research in [26] investigated the relationship between the air flow angle on the brake drum and the cooling effect based on numerical simulations. By systematic simulation, it was found that increasing the angle between the nozzle and the brake drum from 0°C to 15°C could reduce cooling effects and brake rim could lead to tire ablation.

4) Water-Air Cooling System

Another approach is the use of water-air cooling. Scott et al. designed a specific brake rim for water-air cooling in [27]. In this design, a specific brake rim and rotating blade are installed within the brake drum for cooling. The blade rotates and the related vanes inhale air to the brake drum for cooling at the low-speed condition. A temperature sensor is used to measure the drum temperature. If the drum temperature is higher than some threshold value, the water is sprayed into the brake drum. If the temperature is less than the threshold, the control system terminates water flow and switches to air cooling using the rotating blades. However, such a cooling system is expensive and complex in structure for general truck applications.

2.2 Research Objectives

As discussed in the above section, the currently available active brake cooling systems are either insufficient for truck brakes or too complex/expensive to truck applications. Although water cooling is efficient for brakes, the cooling by directly spraying water on the brake drum will definitely reduce the life of the brakes. In addition, these traditional cooling systems are mainly controlled manually or with a low degree of automation. To tackle these related challenges, the objective of this research is to develop an intelligent system for truck brake cooling. This research will use compressed air cooling. Specifically, the proposed intelligent cooling system will have following unique and novel properties:

    (a) A unique air pump with high flow rate will be applied to this air cooling system.

    (b) An intelligent control system will be developed for temperature and water level monitoring and control.

    (c) A new vibration energy harvesting system will be developed to provide battery energy to the cooling system.

2.3 Thesis Structure

After Introduction in Chapter 1 and literature review in Chapter 2 (current chapter), the following summarizes the contents of the remaining chapters in this thesis.

       Chapter 3 provides discussion and some preliminary experimental investigations for brake drum cooling methods.

Chapter 4 presents system analysis of temperature monitoring and brake drum cooling system. It also includes the developed experimental setup of air cooling system.

Chapter 5 contains an overview of energy harvesting systems and the basics in designing piezoelectric energy harvesters.

Chapter 6 systematically discusses the design and analysis of the energy harvesting system. It starts with simulation analysis, followed by the harvester prototype development. The efficiency of proposed energy harvesting system is examined by experimental tests.

Chapter 7 summarizes the concluding remarks and the planned future improvement.

Chapter 3 Preliminary Investigations of Cooling Techniques

3.1 Evaluation of the Related Investigations

Preliminary R&D will be conducted in this chapter to investigate the available ideas so as to develop new concepts and techniques for more efficient brake cooling. Although the objective of this thesis is to develop a brake cooling system with air as medium, the related studies in this chapter will summarize a series of investigations we have undertaken with the use of air as well as water for brake drum cooling. Some important experimental investigation is conducted in terms of distinguishing the time required to cool a brake drum, and airflow rate. The investigation is undertaken under both laboratory and real vehicle testing conditions to provide necessary experience and knowledge in taking advanced R&D in this work.

3.2 Water Cooling Technique

In general, a direct solution for brake cooling would be the use of water, which can increase the heat dissipation rate of brake drums in heavy utility vehicles. A water cooling system has been developed and tested in this work. As shown in Figure 3.1, the developed cooling system consists of two water tanks, a battery power system, a level sensor, a temperature sensor, an automatic controller.

The temperature sensor (model 90614 from Melexis Ltd.) is used to measure the brake drum temperature value and input it to the controller.

Two water tanks are used in this test, one is used for reservoir and another is used to hold the discharged water for circulation.

A water level sensor (model CLA50041 from Xi'an Atech Sensor Ltd.) is used to estimate the water level from water tank. The water level is displayed by the related LED indicators through the automatic controller unit, which includes the following:

Green LED = greater than 60% of the overall height

Yellow LED = 40-60% of the overall height

Red LED = 20-40% of the overall height

Red flashing LED = lower than 20% of the overall height

The water solenoid (model 2W02508 from BOPU Ltd.) is a 12 VDC valve, which can be switched on and off, depending on the control signal from automatic controller.
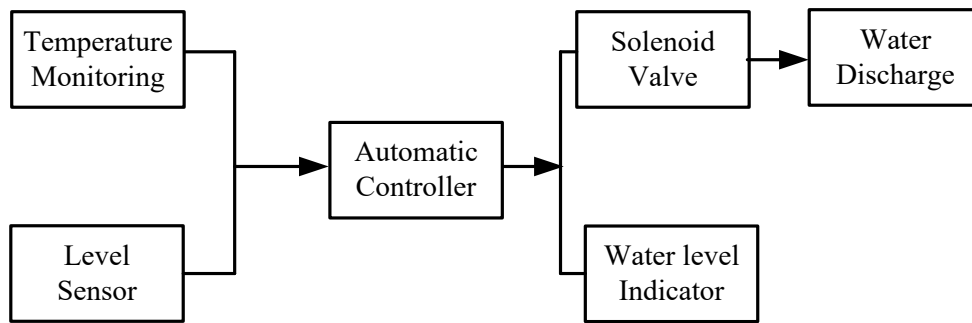
Figure 3.1. Water cooling technique.

The controller is designed with the assistance of another member in my research team. The power to the cooling system is provided by using two 12-volt Nissan 4×4 truck batteries.

In testing, the water reservoir tank is fixed on a frame in the truck bed. The water tank contains about 12 liters of water. Considering the test is taken in winter, the water is circulated to another tank instead of spraying to the truck brakes. A second water tank is located under the reservoir tank to collect water from the solenoid valve. The water level sensor and solenoid valve are installed in the water reservoir tank as shown in Figure 3.2(a).
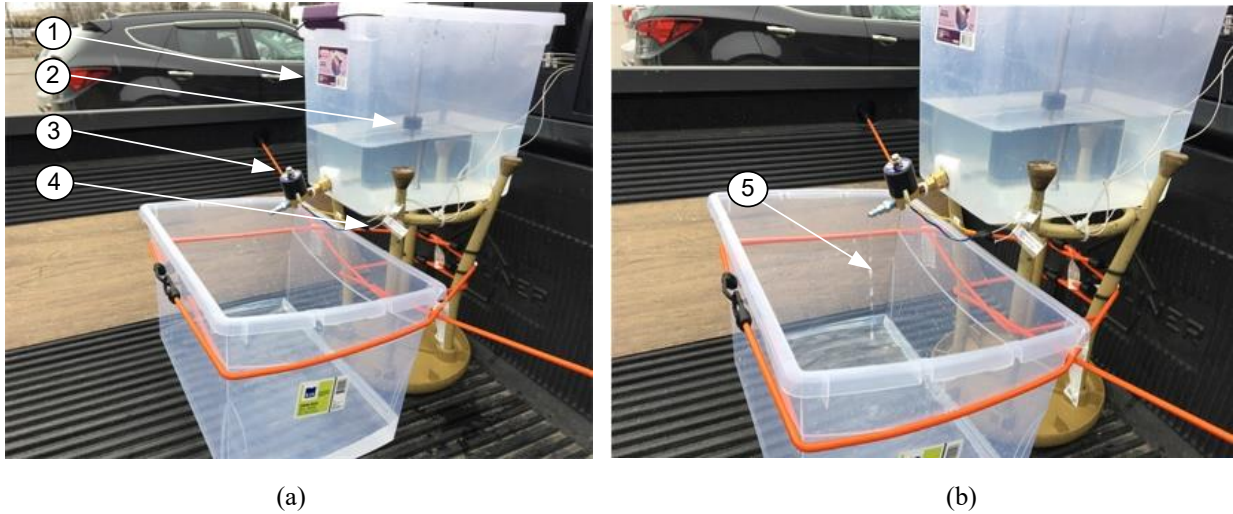
Figure 3.2. Experimental setup for water cooling test: (a) No water output, (b) Water is discharged: (1) Water tank, (2) Level sensor, (3) Solenoid valve, (4) Connections to automatic controller, (5) Water discharged from the solenoid.

One of the purposes of this test is to investigate the cooling performance and the controller robustness while the vehicle is running. In testing, once a threshold temperature is reached (e.g., 150°C), the power to the solenoid valve is on, and water is discharged from the reservoir illustrated in Figure 3.2(b). If temperature is below another threshold (e.g., 100°C), the solenoid will be turned off automatically. In this simulation testing, the threshold value is set to at 30°C, respectively.

From some primary testing, some observations can be obtained.

1) The level sensor output shows a variance in values due to the motion of the vehicle, which creates turbulence in the water level reading. A strategy to improve the robustness of the level of reading could be the use of a level sensor with lower resolutions.

2) The natural water flow rate is low in this experiment. If water is used to cool brakes in real trucks, pressurized air should be introduced to the water tank to keep some pressure on the

surface of the water to increase flow rate. The pressure air could be provided from the high-pressure air tanks for vehicle braking.

3) Water cooling may not be an optimal solution especially in winter season, as water will freeze in the tank. If special liquid with lower freezing point is used, the cost would be increased significantly.

4) Water may generate pollution on the street in cooling brakes. On the other hand, as mentioned in Chapter 2, water cooling could generate the risk of loss of friction between the brake drum and brake shoe, if water accidentally comes into direct contact with the operational surfaces of the brake system.

From the aforementioned investigation, direct water cooling may not be an efficient solution for this project. An air-cooling system will be developed in this work for vehicle brake cooling, as discussed next.

3.3 Air Cooling Technique

3.3.1 Blower Equipment

Firstly, a preliminary attempt is to investigate the use of high airflow from a blower for brake cooling. The blower is a mechanical centrifugal fan, which forces out an air stream for dry cooling applications. Figure 3.3 shows the tested blower (made from Dayton Electric Mfg. Co. Ltd.), which can generate 165.7 CFM (cubic feet per minute) of airflow, powered by 12-volt DC.
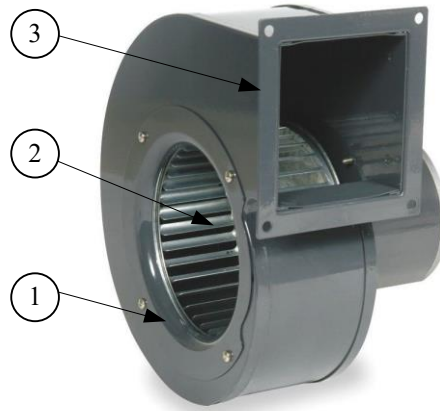
Figure 3.3. The blower model: (1) Air inlet, (2) Centrifugal fan, (3) Air outlet.

Figure 3.4 shows the related experimental setup for this investigation developed by some undergraduate research team. The blower outlet port is converged to a circular duct connector (2.2 inches in diameter). Blower airflow outlet is connected to four different air outlets by use of pipe channels (supposed to cool four brake drums).
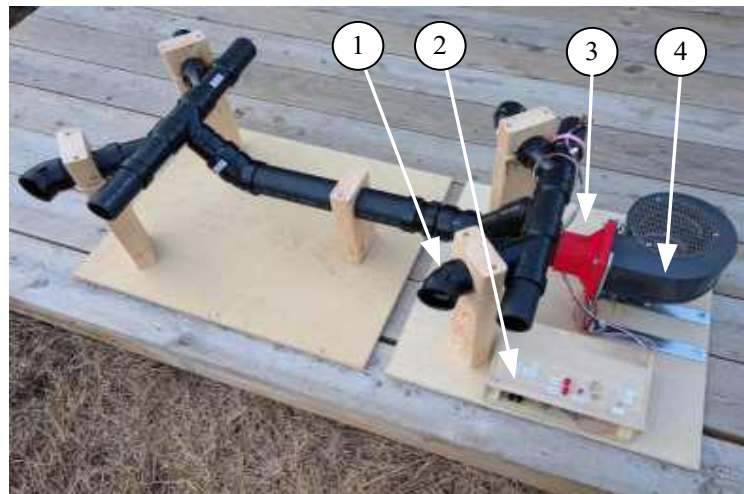
Figure 3.4. The tested blower: (1) Air outlet, (2) Automatic control system, (3) Duct connector, (4) Blower device, (retrieved from [28]).

An automatic controller is designed and used to turn on and off the switch of blower. The temperature sensor is included in the control system, which is to read the simulated temperature variations from a testing plat (to simulate a brake drum). The threshold temperature value is set at

150°C. If temperature rises above this value, the blower is turned on, and it remains on until temperature decreases to 100°C.

From some primary testing, some conclusions can be obtained.

1) Test results show that the 165.7 CFM blower equipment cannot provide sufficient air flow with sufficient flow rate to cool the brake drum.

2) The air flow rate varies with pressure of the blower.

To increase flow rate, a larger blower with 274.7 CFM rate is tested in the cooling system as illustrated in Figure 3.4. Similar problems have been observed as in the 165.7 CFM blower, or the flow rate is sensitive to the pressure and cooling effects cannot meet the cooling requirements in this project. Correspondingly, new solutions have to been found out for this brake cooling project.

3.3.2 Air Compressor-based Cooling Technique

An air compressor is a device that is designed to compress air to a higher pressure. Air compressors are categorized into two types: rotary screw form and reciprocating mode [29]. as illustrated in Figure 3.5. The rotary screw compressor uses a rotary-type positive-displacement mechanism. The air is compressed when two rotary screw components' continuous circular movement inhale air inside a void space as shown Figure 3.5(a) [30]. A reciprocating air compressor uses pistons driven by a crankshaft to deliver gases at high pressure as illustrated in Figure 3.5(b). This type of compressor is commonly used in automobile and air conditioning applications. A characteristic of reciprocating compressors is that the flow output remains nearly constant over a range of discharge pressure. Reciprocating compressors are powered by either an internal combustion engine or an

electric motor. The electric powered reciprocating compressor is considered in preliminary investigations. In electric air compressor is powered through induction motor. Electric motor-powered reciprocating compressors are considered in this preliminary investigation.
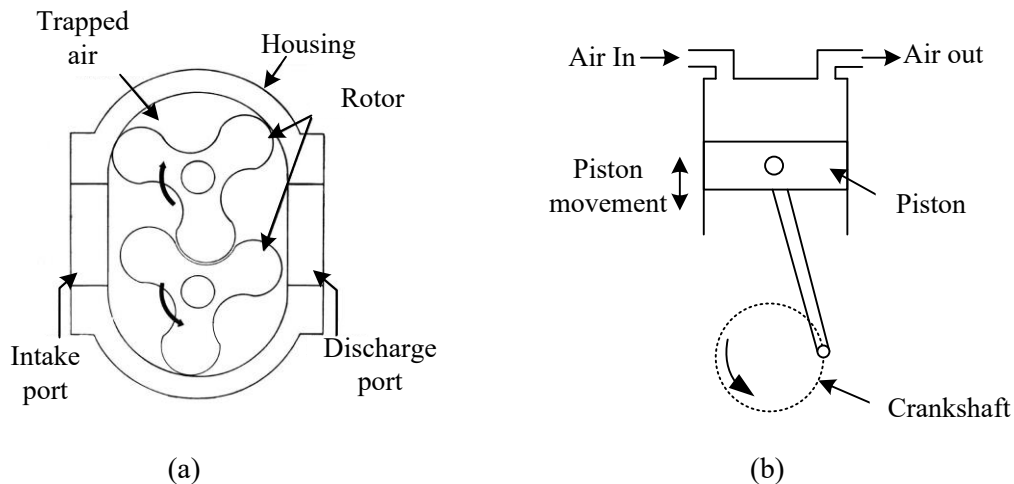
Figure 3.5. The schematic diagrams of (a) Rotary screw air compressor, (b) Reciprocating air compressor (retrieved from [29]).

1) The Cooling System Using an Inflator

An inflator is small, low-powered air compressor. It is capable of producing up to 110 psi (pounds per square inch) of air pressure with low power consumption. Inflators are used mostly for inflating automobile tires. The inflator (model HD12120 from Husky Ltd.) is tested in this work to analyze airflow output, as illustrated in Figure 3.6. This inflator model can operate on 12 VDC supplied from a battery, or on 120-volt AC power outlet. An anemometer device is used to measure the airflow rate. The airflow rate from the outlet pipe is measured by using the anemometer, as shown in Figure 3.6.
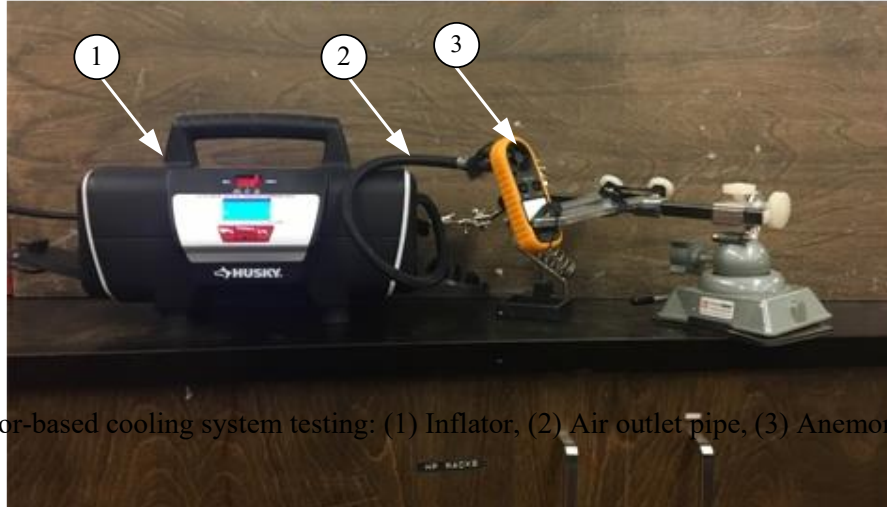
Figure 3.6. Inflator-based cooling system testing: (1) Inflator, (2) Air outlet pipe, (3) Anemometer.

The maximum airflow rate under the tested operating condition of the inflator is 1.25 CFM, which is not enough to cool more than one-wheel drum. The studies have confirmed that although the inflator can provide air high pressure (e.g., up to 150 psi), its airflow rate is not enough for this brake cooking purpose.

2) Air Compressor Equipped with Air Tank

In general, an air tank is equipped with a compressor to keep the air up to some pressure level. A high pressure configured air compressor is selected to analyze airflow performance. The compressor (model 058-1292 purchased from Maximum Ltd.) is applied for the experiments, as illustrated in Figure 3.7. The airflow is measured using the anemometer at pressure valves. The compressor is operated with a 120-volt AC power supply. By systematic testing, the airflow rate is noted as 2.852 CFM at 40 psi and 1.94 CFM at 90 psi, respectively. The power consumption of this air compressor model is observed as 1.20 HP.
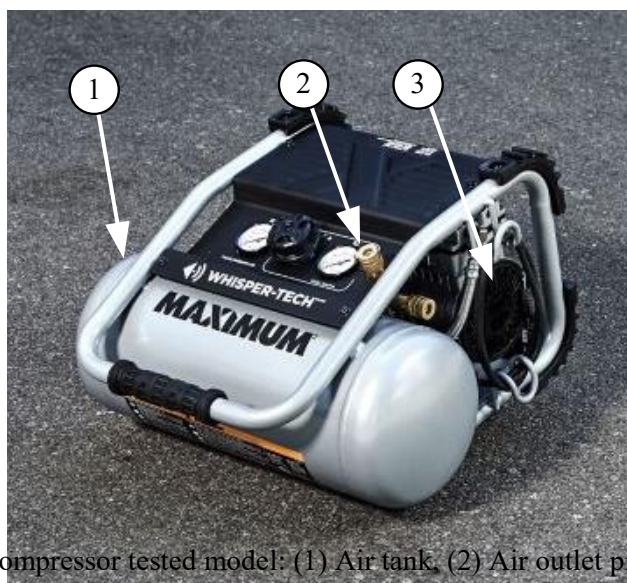
Figure 3.7. The 120-volt air compressor tested model: (1) Air tank, (2) Air outlet pipe, (3) Air compressor cylinder.

The following observations can be obtained after experimental testing:

1) In order to achieve sufficient airflow rate for brake drum cooling, more power consumption is needed.

2) The experimented compressor model is equipped with a 15.1 Litre air tank, which makes it heavier.

3) The available voltage on a heavy-duty utility vehicle is 12 volts or 24- volts. Therefore, the tested compressor (a general industrial one) cannot be installed on a truck because this air compressor requires a 120-volt DC power supply.

3) Double Air Compressor-Solution

To increase air flow rate, two air compressors are used for this project to cool a brake drum. Two air compressors (model 420C from Viair) are tested using a 12 VDC power supply, as illustrated in Figure 3.8. The analysis is in terms of airflow rate and power consumptions. Based on the test results, the pair of Viair compressor setup can provide flow rate of 4.85 CFM, at a pressure of 20

psi. The power consumption of this setup is 0.75 HP (horsepower). Although the air compressor setup has demonstrated impressive output results with regards to airflow requirement, it still could not meet the brake drum cooling requirements. Furthermore, during the operation of this setup, both compressors would turn off automatically due to an overheating problem of its drive motors, or these pumps are not supposed to be used for continuous cooling applications. However, these results raise the possibility of using a dual-cylinder air compressor in the brake drum cooling system.
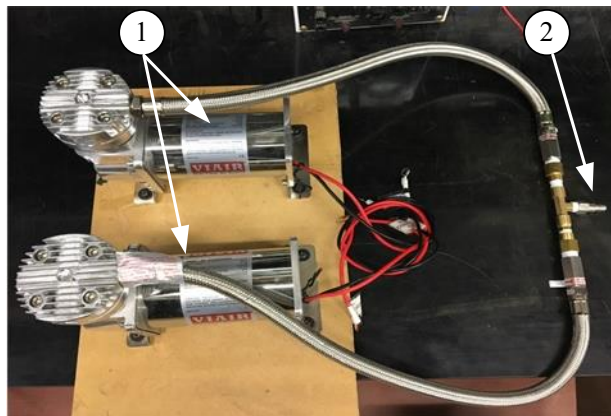
Figure 3.8. 12-volt DC dual air-compressor tested system: (1) Two air compressors, (2) Combined air outlet port.

3.4 A Newly-designed Air Compressor

Although preliminary testing of the standard air compressors available in the market has shown some cooling effects, they cannot provide sufficient high airflow rate that is required for cooling purposes. The design and fabrication of the custom air compressor is a reasonable solution to this problem. The new air compressor is designed to fill the airflow demand of a brake drum cooling system application [31]. The new air compressor will be designed in considering some specific requirements: low power consumption (e.g., less than 0.65 HP) and high airflow rate (e.g., up to 8 CFM). The following procedure summarizes the related design processes.

1) Calculate compression ratio (R)

$$R = \frac{P_d}{P_s} \qquad (3.1)$$

where P_d and P_s are the discharge pressure and suction pressure (bar), respectively. For example, if P_d = 3.447 bar and P_s = 0.992 bar, R = 3.474.

2) Choose stages of the compressor

With respect to the calculated value of R = 3.474, from Table 3.1, it appears that a single cylinder or a two-stage unit can meet this requirement.

Table 3.1 Chart for choosing the proper number of stages [31]

R-Value	Number of Stages
1-3	single-stage
3-5	normally single-stage, occasionally two-stage
5-7	normally two-stage, occasionally single-stage
7-10	two-stage
10-15	usually two-stage, occasionally three-stage
15+	three-stage

Considering the output requirement of an air compressor, from Table 3.2, a two-stage compressor is determined to be the appropriate choice. A lower discharge air temperature is acceptable for an air cooling system application with low power consumption.

Table 3.2 Comparison of single-stage and two-stage compressor [31]

Parameters	Single-Stage	Two-Stages
Discharge temperature	higher	lower
Brake Horse Power (BHP)	higher	lower
Initial cost	lower	higher
Overall system complexity	lower	higher

3) Calculate the discharge temperature (T_d)

$$T_d = T_s R^{\frac{(n-1)}{n}}$$ (3.2)

where T_d and T_s are the discharge temperature and suction temperature ($^\circ$K), respectively, and n is the specific heat ratio of gas. The compressor's discharge temperature affects the life of the piston rings and valves. Keeping values as $R=3.474$, $T_s = 305.15^\circ$K, and $n = 1.4$ in (3.2) formula, $T_d = 435.54\,^\circ$K.

If the calculated temperature is higher, the study recommends a two-stage compressor model [32]. Additionally, selection of two-stage compressor is mainly used in air conditioning purpose, consumes low power to operate.

4) Calculate the volumetric efficiency (*VE%*)

$$VE\% = 89 - R - 7.8 \left(R^{\frac{1}{2n}} - 1 \right)$$ (3.3)

where n is the specific heat ratio of gas. The volumetric efficiency is used to evaluate the amount of compressed gas versus the physical size of the compressor's cylinder volume. Substituting $R = 3.474$ and $n = 1.4$ values in Equation. (3.3), the volumetric efficiency $VE\% = 81.2\%$.

5) Compute the actual piston displacement (PD)

$$PD = \frac{BHP}{0.00528\left(\frac{n}{n-1}\right)(P_s)\left(R^{\frac{n-1}{n}} - 1\right)} \tag{3.4}$$

where PD is actual piston displacement in CFM, n is the specific heat ratio of gas, BHP is brake horsepower (HP), and P_s is suction pressure (bar). Because actual piston displacement is the intake of airflow inside the cylinder, the unit of piston displacement is measured in CFM. If $R = 3.474$, $n = 1.4$, $P_s = 0.992$ bar $= 14.69$ psi, $BHP = 0.65$ HP, then $PD = 5.60$ CFM.

6) Calculate the dimension of the air compressor cylinder. The desired flow rate in CFM will be

$$CFM_d = V_{cylinder} \times RPM \tag{3.5}$$

where RPM denotes the rotating speed of the induction motor. $V_{cylinder}$ is the volume of the cylinder, $V_{cylinder} = \pi r^2 h$, where r and h are the radius and the height of the cylinder. In this case [33], if the $CFM_d = 8$ and $RPM = 1550$ then diameter of cylinder is selected as $d = 2\,\frac{3}{4}$ inch, the height of the cylinder will be $h = 1.356$ inch.

7) Determine the stroke length of the piston

An air cylinder compresses air in response to movement of the reciprocating piston [34]. The distance that the piston travels is called the length of stroke, which is directly related to the capacity of the reciprocating compressor. In this case, the length of stroke can be calculated as,

$$l = \frac{V_{cylinder}}{\pi . \left(\dfrac{d}{2}\right)^2 . c} = \frac{\pi r^2 h}{\pi . \left(\dfrac{d}{2}\right)^2 . c} \tag{3.6}$$

Substituting the selected and calculated values $d = 2\frac{3}{4}$ inch and $h = 1.356$ inch, $c = 2$ (number of cylinder), from Eq. (3.6), the piston stroke length $l = 0.687$ inch.

The overall design parameters of the air compressor are listed in Table 3.3

8) Design the ventilation of electric induction motor

Electric motors generate heat as a result of the electrical and mechanical loss inside the electric machine. The generated heat should be dissipated properly; otherwise overheated motor will affect both motor reliability and performance efficiency [35]. As a matter of fact, some unexpected stoppage during experimental testing of air compressors is observed due to poor ventilation.

The external frames of the motor are usually provided with cooling fans to increase heat ventilation. The cooling fan is made of a strong plastic material, aluminum, or steel. The cooling fans are generally mounted on the rotor shaft of the induction motor. In design consideration of new compressor, cooling fans are provided on both sides of the compressor.

Table 3.3 Estimated values for two-stage compressor

Design Parameters	Determined Values
Compression ratio (R)	3.474
Stages	2
Discharge temperature (T_d)	435.54 °K
Volumetric efficiency ($VE\%$)	81.15%
Actual piston displacement (PD)	5.60 CFM
Diameter of cylinder (d)	2 ¾ inch
Height of cylinder (h)	1.356 inch
Stroke length of piston (l)	0.678 inch
Ventilation of induction motor	2 Cooling fans
Expected airflow out (CFM_d)	8 CFM

3.5 The New Air Compressor System

Based on the related design parameters, a specific air compressor has been designed in this research team and a prototype has been fabricated by a contractor in China for this work, as shown in Figure 3.9. The designed air compressor has two cylinders at both ends of the compressor. Two-stage cylinder arrangement helps improve the flow of air and. The motor has 0.6 HP, and 24 VDC. Two fans are installed to both sides of compressor shaft to keep the compressor cylinders from overheating.
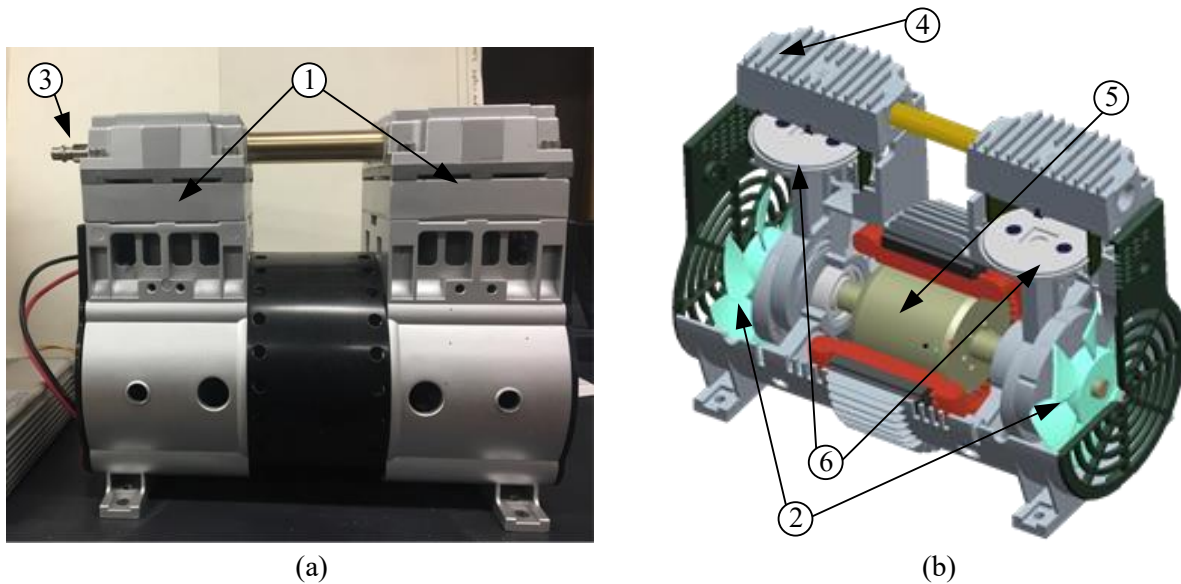
Figure 3.9. Designed air-compressor: (a) Manufactured air compressor, (b) 3D drawing model: (1) Two cylinders, (2) Two cooling fans, (3) Inlet port, (4) The outlet port side, (5) Air-compressor motor, (6) Two pistons.

The performance of the new air compressor is verified by using experimental testing setup shown in Figure 3.10. Two 12-volt batteries are connected in series to provide 24 VDC. This specially designed air compressor can discharge from 7.5 to 8 CFM of airflow through the outlet port, which is much higher than commercially available air compressors. Based on this new air compressor, detailed intelligent cooling system design will be discussed in the following chapter.
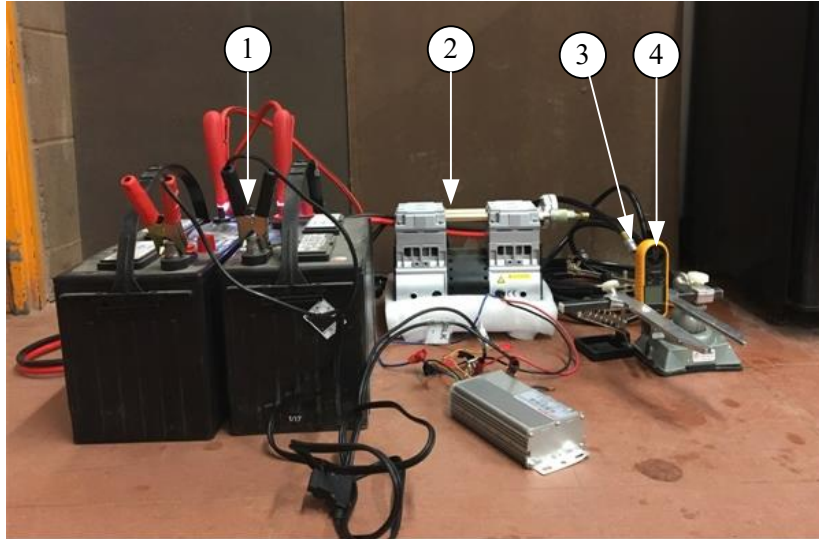
Figure 3.10. Testing setup for the designed air-compressor: (1) 24-volt battery source, (2) The new air compressor, (3) Outlet port, (4) The anemometer.

Chapter 4 The Development of the Air Cooling System

4.1 System Analysis

Appropriate cooling is essential to maintain brakes within acceptable operating temperature levels. According to the literature review and preliminary investigations in Chapter 3, an intelligent air cooling system will be developed in this work. As illustrated in Figure 4.1, the developed intelligent cooling system includes the units of temperature monitoring, controller, air compressor, and air transmission channel.

Temperature Monitoring	→	Automatic Controller	→	Air Compressor	→	Air Transmission
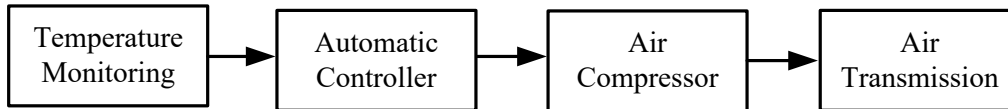
Figure 4.1. The basic block diagram for intelligent brake cooling system.

For an air cooling system, the prime part is the air source. The air should have some pressure to overcome transmission resistance and improve cooling efficiency. Although the vehicle has a high-pressure air source generated by an air compressor with pressure 150-200 psi, this high-pressure air source is mainly used to apply the pressure to brake pads to slow down or stop the vehicle. This high-pressure source may not be useful for the developed cooling system. Firstly, there could be a functional conflict when the vehicle is in braking operation, and the cooling system is still working, such as the case in downhill driving. Secondly, the vehicle braking air system requires high pressure but low flow rate, however, our developed air-cooling system requires low pressure but high flow rate. Therefore, it is not appropriate to use the high-pressure source in the vehicle for the developed air-cooling system. On the other hand, there are no air compressors in the market, which can meet our high flow rate but low-pressure requirements. Correspondingly, a specific air compressor has been designed, as discussed in Subsection 3.5.

31

4.2 The Intelligent Control System

An electric control system is designed by our research team to control the cooling process [36]. Control system is to generate the desired output based on the input information. The intelligent control controller should have the capability to act properly under a noisy environment, and to achieve a high degree of autonomous behavior [37]. Figure 4.2 represents the schematic of the control system and its hardware components. This system consists of a temperature sensing unit, the micro-controller unit, the motor switching circuit, and the compressor motor.
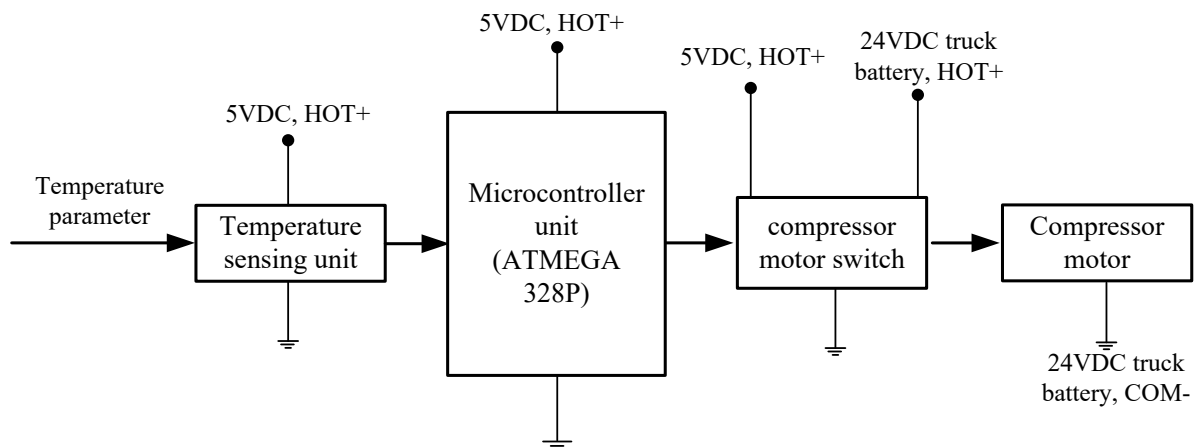
Figure 4.2. The control system schematic diagram.

4.2.1 Temperature Sensing Unit

Temperature can be measured either directly from the heating source or remotely without direct contact with the source. In this specific cooling system, the brake drum temperature will be measured remotely by using an infra-red (IR) temperature sensor (model 90614 from Melexis Ltd.) as shown in Figure 4.3(a). This non-contact IR sensor has properties of measurement range from -70ºC to 380ºC, measurement accuracy of 0.5ºC and resolution 0.02ºC, which are suitable for this temperature measurement requirements. Figure 4.3(b) is an experimental model of the temperature

sensor with a pinboard. It is powered by a 5-volt DC power supply. Temperature sensor output is sent to the microcontroller unit for cooling system control.

<div align="center">(a)   (b)</div>

Figure 4.3. Diagrams of (a) IR temperature sensor, (b) Temperature sensor with pinboard (retrieved from [38]).

Figure 4.4 represents the schematic of IR temperature sensor input to the microcontroller unit. The temperature sensor is powered through VCC (common voltage connector) and VSS (voltage source supply) pin connection. The VCC pin is used for positive terminal connection, and VSS is noted for negative terminal connection with a power source. Temperature data is transmitted to the microcontroller unit by SDA (serial data) and SCL (serial clock) lines, pulled up with resistors. These lines are connected with two resistors to limit the flow of current. Additionally, the decoupling capacitor is connected in parallel to the power supply of sensor. Two resistors can supply smooth power to temperature sensor without interruptions.
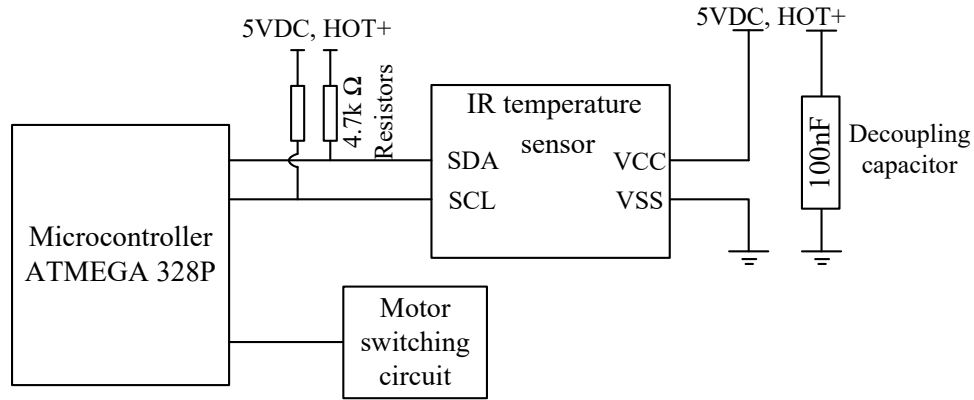
Figure 4.4. Schematic of IR temperature input to the microcontroller unit.

4.2.2 Microcontroller Unit

The microcontroller unit is the core part of this cooling control system. The functions of the microcontroller are to store data, process data, and generate control signals to the manipulated system such as a compressor motor in this case. In this work, ATMEGA 328P microcontroller (from Atmel® AVR® Ltd.) is selected due to its low power consumption, high-performance configuration, and availability of reference resource codes. ATMEGA 328P has a 32 Kbytes in-system programmable flash memory, external oscillator maximum speed rate of up to 20 MHz, selectable 28 pins, 2 Kbytes of SRAM data memory, and an arithmetic logic unit to run program code [39]. Figure 4.5 shows the schematic of the microcontroller unit. The control system takes input from measured temperature data and processes this data through embedded programming code. The microcontroller generates the control signal to the compressor motor through to the switching circuit.
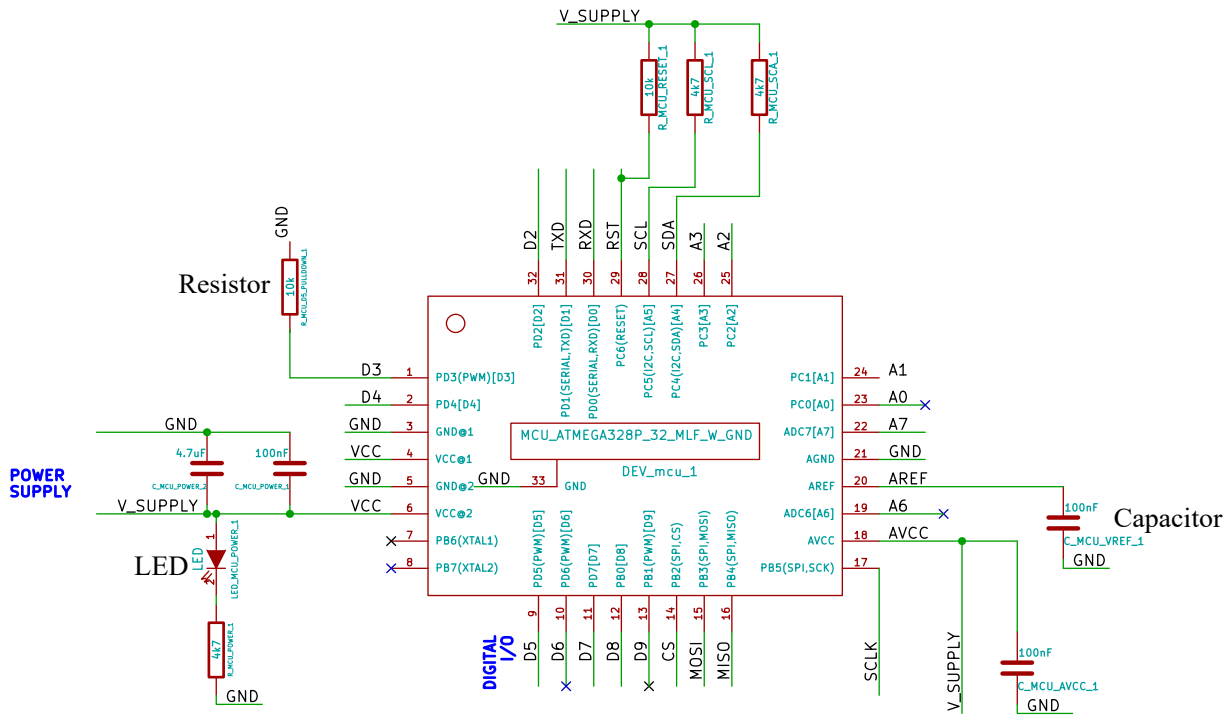
Figure 4.5. Schematic of the microcontroller unit [36]

The microcontroller circuit requires some auxiliary electronic components such as resistors (4.7kΩ and 10kΩ configured), capacitors (4.7nF and 100nF configured) and LED light. In the circuit, 4.7 kΩ configured resistors are connected with signal lines as pulled up resistors, which are used to ensure a well-defined logical level (high or low) at the related pins under all conditions. In this microcontroller circuit, the 4.7 kΩ resistor is used to make the signal line at the high logic level. Furthermore, the 10 kΩ resistor is used to enable steady state or reset function of the microcontroller. Whenever the power goes above or below specific voltage value, the 10 kΩ resistor resets the value of the microcontroller pin. Capacitors (4.7nF and 100nF configured) are used to store charge in the microcontroller unit. The immediate supply of the current to the microcontroller circuit can be accomplished by connecting the capacitors [40]. The LED component is used to indicate microcontroller status in the circuit. For example, if the LED is on

then microcontroller circuit is in an active state. The fabricated microcontroller circuit board is showed in Figure 4.6.
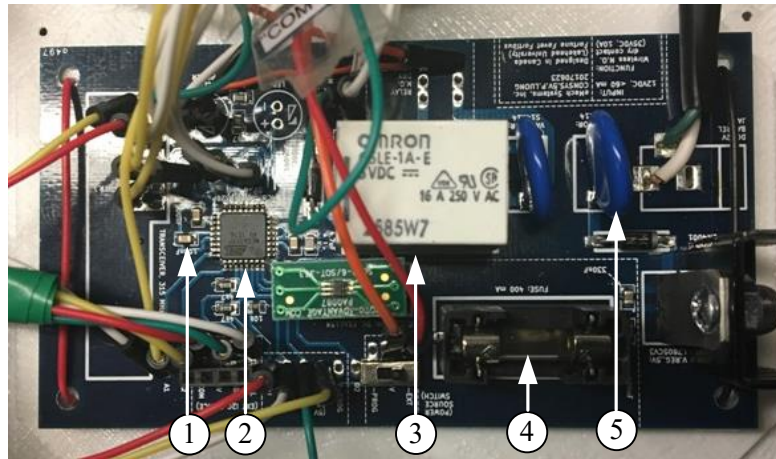
Figure 4.6. Fabricated microcontroller circuit board [36]: (1) Capacitor, (2) ATMEGA 328P, (3) Relay #1, (4) Fuse, (5) Varistor.

Figure 4.7 illustrates system control procedures. In operation, if the measured temperature is above a threshold value (e.g., 150°C), the air compressor is turned on. Then airflow from the compressor is guided to the wheels to cool the brake drums. If the temperature is below another threshold (e.g., 100°C), the air compressor motor is turned off.
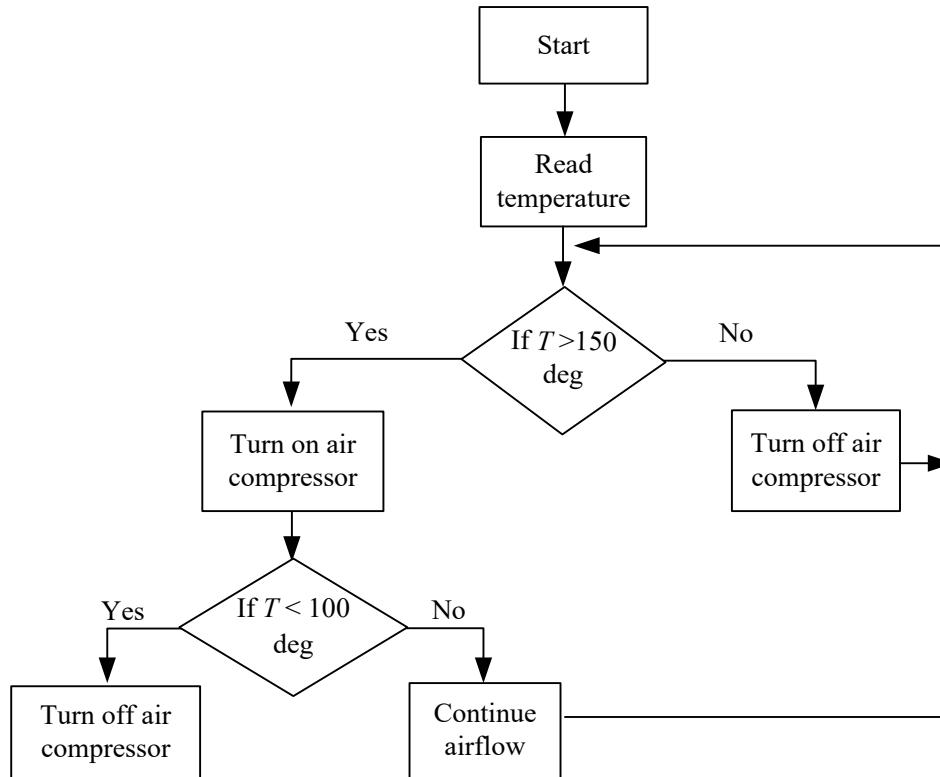
Figure 4.7. Flowchart for control system analysis.

The microcontroller controls the air compressor motor by use of a switching circuit as discussed next.

4.2.3 The Motor Switching Circuit

The motor switching circuit is to handle the high voltage power required to operate the compressor motor, based on the control signals from the microcontroller. The motor switch circuit will have appropriate response time to ensure that the power applied to the motor can be applied and removed precisely. The motor switch circuit consists of a digital switch and two relays, as illustrated in Figure 4.8. It is an electrically operated switch circuit with no moving components, which can isolate circuit and control a significant amount of power using a small control signal. Compared with electromechanical switch, a digital switch can operate much faster and over much longer

extended periods without wearing out conditions. Typically the time period from applying a command signal to turning on the output circuit is about 20 microseconds only. The digital switch (model FSA1156P6X from Semiconductor Ltd.) is selected in this control system. A digital signal from the microcontroller triggers the digital switch to initiate low current flow through the circuit. In this motor switching circuit, a small current input (e.g., 200 mA) to the digital switch can turn on two relays simultaneously. The switch circuit can also allow a high current to flow from the battery source to the compressor motor.
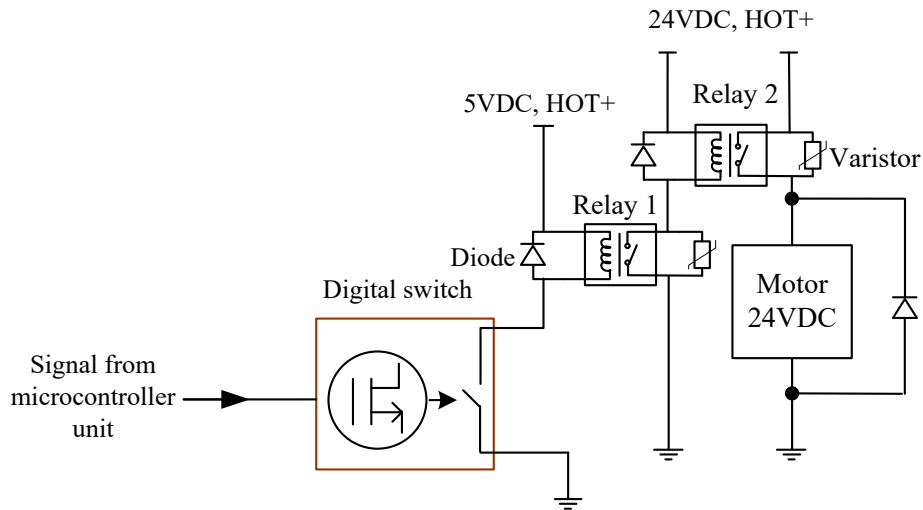
Figure 4.8. Schematic of solid state switching circuit

The compressor motor requires a 24VDC power supply. Due to relatively high voltage and current, a single relay may be insufficient to work properly over a long time period. To improve reliability, two relays (model V23134B1 from EV-CBOX Ltd.) are used in this motor switch circuit. Primarily, the relay is an electromagnetic device that can be actuated by an electrical current. A relay is a remote control switch, and is generally open contact when it has no input. When power is applied to the coil inside the relay, a magnetic field is created to close the switch. A diode (model 1N4001from Rohs Ltd.) is connected to both relays to ensure the electric current follows in one direction only. The diode provides a path for current when the coil is switched off,

otherwise a voltage spike could occur and cause arching on switch contact. In the motor switching circuit, the digital switch generates current through relay #1, which in turn actuates relay #2. Relay #2 will allow power to be supplied to the compressor motor. Additionally, a varistor (model S14K14 from TDK Ltd.) is connected to each relay to ensure that if the voltage suddenly exceeds a predetermined value, the varistor becomes short-circuit to protect the relay circuit. The varistor in relay #2 can also protect the circuit from truck battery voltage spikes.

Figure 4.9 illustrates the developed primary control system hardware as per above-illustrated information.
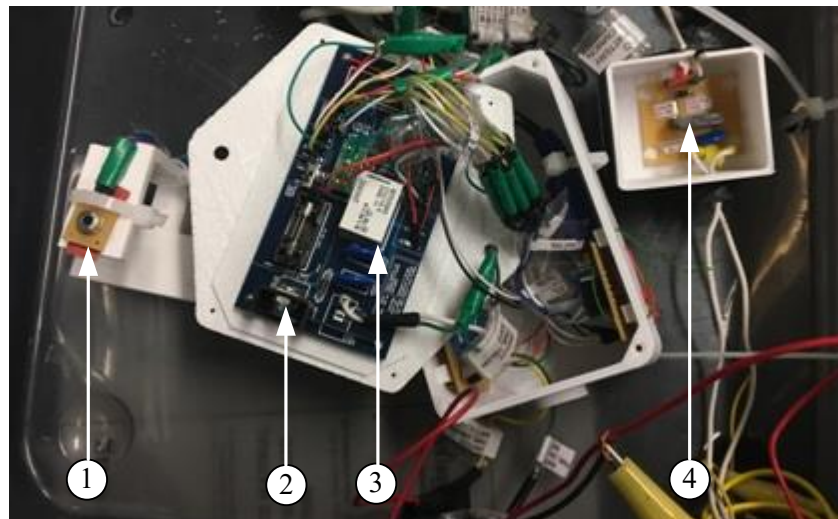
Figure 4.9. The developed primary control system hardware: (1) Temperature sensor unit, (2) Microcontroller unit, (3) Relay #1, (4) Compressor motor relay #2.

4.3 Experimental Setup

The experimental setup used in this research is shown in Figure 4.10. Two 12V batteries are connected in series to provide 24V voltage for the air compressor. The temperature sensor is fixed to the testing system to read brake drum temperature. A used brake drum from Maxim Truck Ltd. is used for this experimental test. The brake drum is properly supported in such a way that cooling

can be performed on the outside of the brake drum. A propane torch is used to heat the brake drum to the desired temperature level for testing.
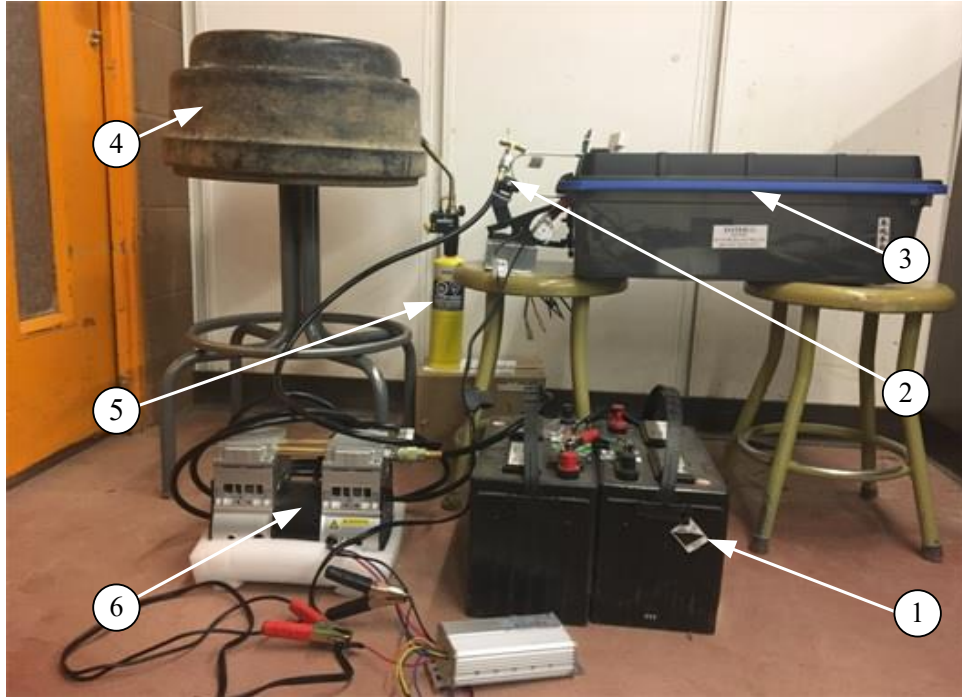
Figure 4.10. The automatic brake drum cooling schematic setup: (1) 24-volt battery, (2) Airflow outlet with T-shape connector port, (3) Electronic control system, (4) Brake drum, (5) Heat torch, (6) Air compressor.

An electronic control unit is used to regulate the flow of air from the compressor onto the brake drum. A *T*-shape connector as represented in Figure 4.11 is used at the end of the airflow outlet pipe to replicate air flow onto two wheels (one is used in this test). The measured airflow on both sides of the outlet port is approximate 3.8 CFM.
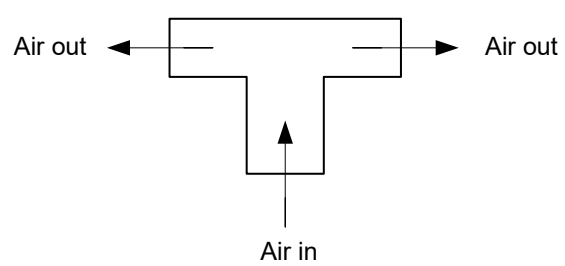
Figure 4.11. A *T*-shape connector.

4.4 Experimental Tests

4.4.1 Experimental Procedures

Several tests have been performed to test the efficiency of the cooling system. The test results are evaluated in terms of the time required to decrease the temperature from 150°C to 100°C and from 200°C to 100°C, respectively. Three test conditions are considered:

    1) Natural Cooling: The brake drum is heated to a higher temperature, for example, 150°C or 200°C. Then let it cool naturally without using the developed cooling system. The cooling time is recorded up to the drum temperature drops to 100°C via natural convection.

    2) Natural Cooling with a Constant Heat Source: The test conditions are the same as in "Natural Cooling" except the heater remains on during the cooling process.

    3) Forced Cooling: The brake drum is heated to reach 150°C or 200°C, and then the heater is removed, and the brake drum is cooled by using the developed air cooling system.

    4) Forced Cooling with a Constant Heat Source: The test conditions are the same as in the "Forced Cooling" except the heater remains on during the cooling process.

4.5 Test Results Analysis

Many tests have been conducted with the above conditions. The following are some typical examples for each test conditions. Figure 4.12 shows the test results of the drum with the natural cooling and the forced cooling using our developed cooling system. It is seen that the developed cooling system can provide more efficient cooling effect than the natural cooling. The time

required to cool from 150°C to 100°C is observed as 30.15 seconds for the forced cooling versus 179 seconds for the natural cooling condition.
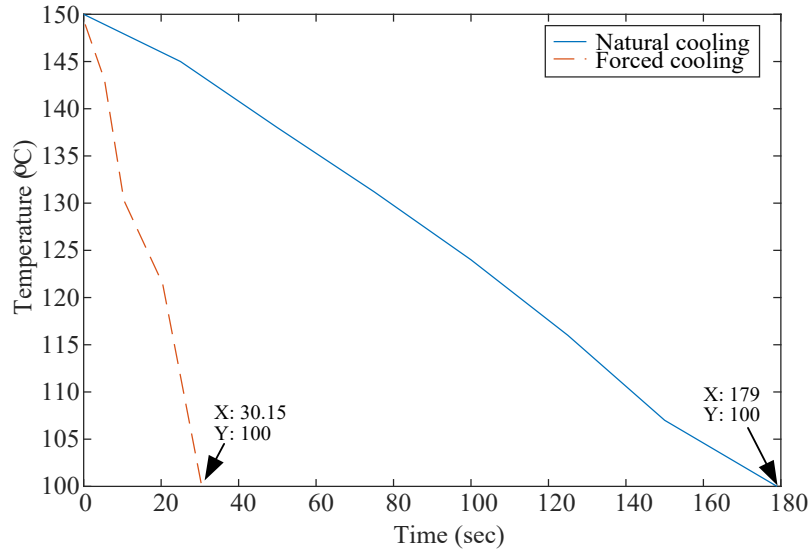
Figure 4.12. Brake drum cooling from 150°C to 100°C with the heater off.

Figure 4.13 shows the comparison of the testing results starting at 200°C. The developed cooling system takes 70 seconds to decrease the temperature from 200°C to 100°C, while the natural cooling takes about 206 seconds to reach the same cooling effect.
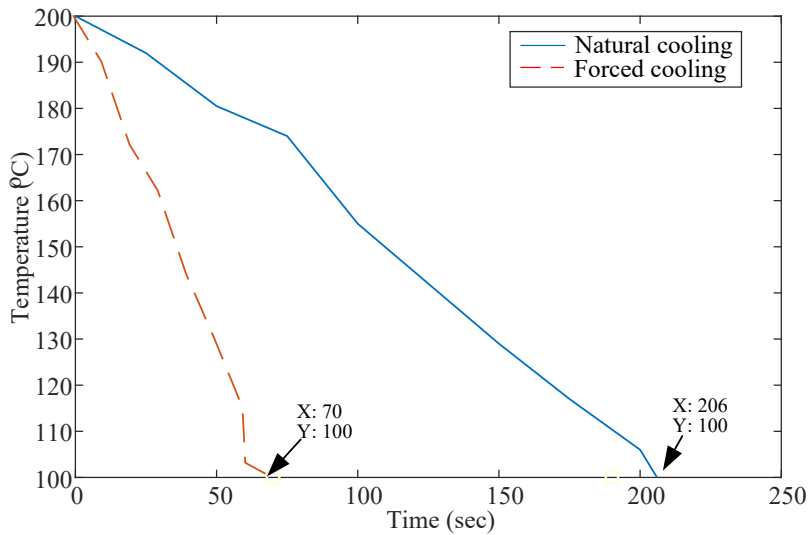
Figure 4.13. Brake drum cooling from 200°C to 100°C with the heater off.

Next, cooling effects are compared for conditions when the heater keeps on during the cooling processes. Figures 4.14 and 4.15 show the cooling performance comparison using the proposed active/forced cooling and the natural cooling, corresponding to the starting drum temperature at 150°C and 200°C, respectively. It is seen that in both cases, the natural cooling could not reduce the drum temperature as the system in thermal equilibrium. The developed active cooling can effectively reduce temperature of the drum; it takes about 150 seconds to cool the drum from 150°C to 100°C, and takes about 190 seconds to decrease the drum temperature from 200°C to 100°C. In summary, these test results can demonstrate the effectiveness of the developed air cooling system.
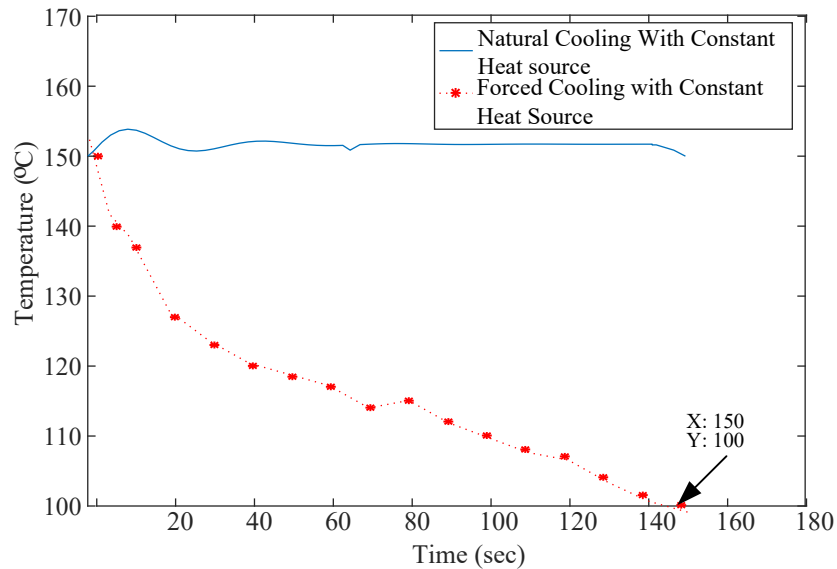
Figure 4.14. Brake drum cooling from 150°C to 100°C with the heater on.
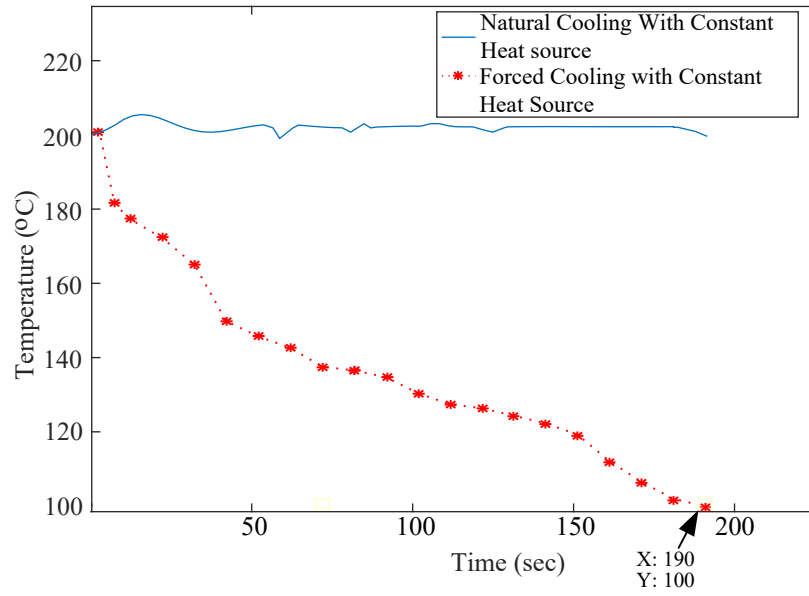
Figure 4.15. Brake drum cooling from 200°C to 100°C with the heater on.

Chapter 5 Fundamentals of Energy Harvesting System

5.1 Overview

The purpose of the development of an energy harvesting system is to harvest the vibration energy in a moving vehicle into electrical energy so as to power the smart temperature sensors. Energy harvesting can be based on several types of energy sources such as thermal energy, solar energy, wind energy, and vibration [41]. In thermal energy harvesting, the heat flux (i.e., temperature differential) is converted into electricity. But the major drawback of thermoelectric system is related to maintaining a continual temperature difference in applications. The solar energy harvesting systems generate electrical power from sunlight by use of solar cells [42]. But the initial cost of a solar cell setup is expensive. The wind energy harvesting applies wind turbines to convert the kinetic energy imparted by wind to electric power. Wind turbines are typically located at sites with sufficient winds, and usually in some remote areas [43]. Vibration energy harvesting is to convert ambient vibrations from sources such as vehicles, bridges and human motion, to electrical energy [44]. In this project, the purpose is to charge batteries for smart sensors, with very low power level in contrast to the conventional energy sources that drive high power consuming devices. Correspondingly, a small scale but efficient vibration harvester will be developed in this work. A vibration piezoelectric energy system will be used as the energy harvesting transducer.

The new energy harvesting system is proposed to generate power from the ambient vibration of the vehicle. As shown in Figure 5.1, the energy harvesting system includes main component such as piezoelectric transducer, interface circuit and battery. The Piezo-electric transducer converts vibrational energy to electrical energy due to its material property (discussed in subsection 5.2.1). The interface circuit component is simplified circuit (discussed in section 6.6)

to charge the battery. Furthermore, this charged battery power can able to supply power to temperature sensor of cooling system.
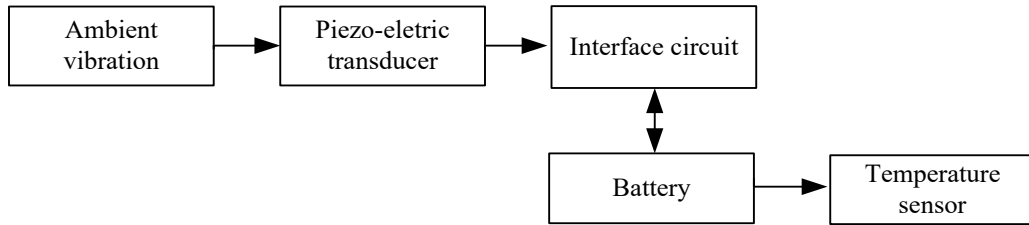
Figure 5.1. The block diagram of the proposed energy harvesting system.

5.2 Piezoelectric Energy Harvester

5.2.1 Basic Piezoelectric Material

Piezoelectric energy harvesting uses piezo elements to convert the kinetic energy from vibrations or shocks to electrical energy [45]. The word "piezoelectric" is derived from the Greek piezein, which means to squeeze or press, and piezo means "push". The piezoelectric phenomenon is a reversible physical process that occurs in certain materials including quartz, berlinite, sucrose, and lead titanate, etc [46]. The lead titanate material is specifically useful for low-frequency vibration applications, which will be applied for this work.

Piezoelectric materials can be categorized as unimorph and bimorph, which have one active layer and two active layers, respectively [47]. The bimorph configuration with active circuitry is more commonly used in the field of vibration energy harvesting, which is also used in this work.

5.2.2 Piezoelectric Crystal Functionality

Piezoelectricity is generated from the deformation of the stable condition of atoms under mechanical stress. In general, crystalline materials contain regular and symmetrical atomic

structures, where every atom is differentiated by possessing some positive or negative charge [48]. Under normal conditions, positive charges cancel negative charges, which results in a material with a balanced neutral charge state, and positive and negative charge are equally distributed, as illustrated in Figure 5.2(a).

<div align="center">(a)   (b)   (c)</div>
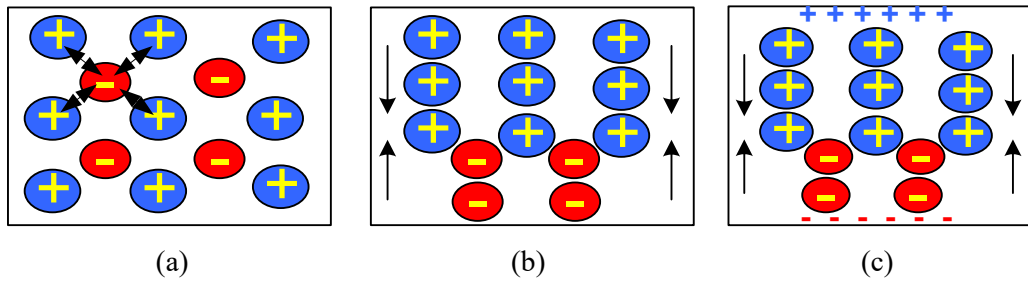
Figure 5.2. Piezoelectric structure: (a) Balanced state, (b) Under mechanical stress (compression), (c) Piezoelectric effect.

When a piezo material is under mechanical stress (compression or stretching), the charge distribution is violated as shown in Figure 5.2(b), resulting in positive and negative charges to migrate to opposite sides of the crystal. Consequently, piezoelectricity is generated across the piezo-material as illustrated in Figure 5.2(c).

5.2.3 Piezo-material Modes

Piezo-materials have two unique properties: the direct piezoelectric effect and reverse-piezoelectric effect. As illustrated in Figure 5.3, in the direct piezoelectric effect, mechanical stress or force is applied vertically or axially on a piezo material, which generates a voltage across the poles. Figure 5.4 depicts the reverse piezoelectric effect, where the expansion (or compression) is created by applying an electrical voltage across piezo-material [47].
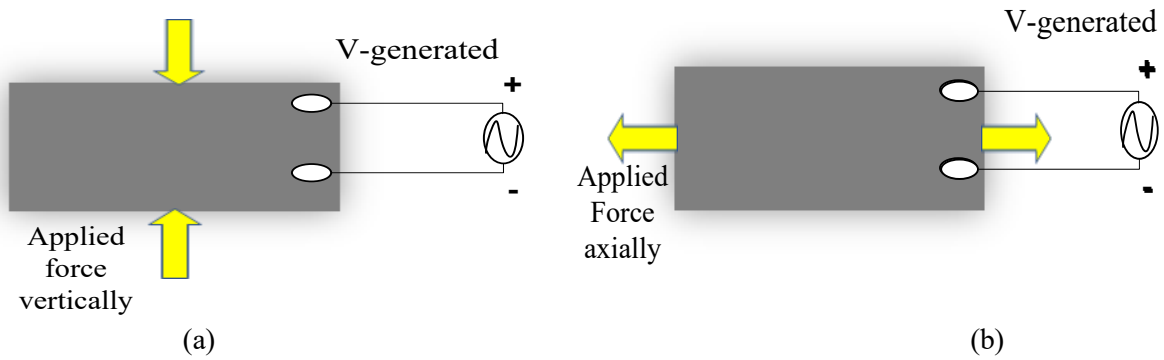
Figure 5.3. Direct-piezoelectric effect: (a) Applied force vertically, (b) Applied force axially.
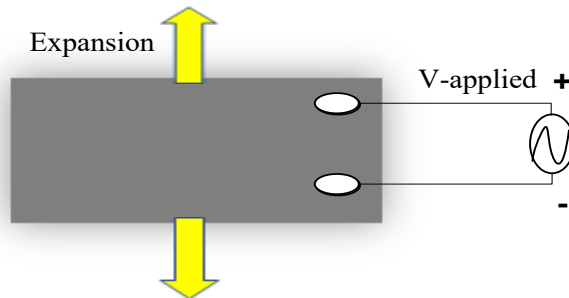
Figure 5.4. Reverse piezo-electric effect.

5.3 The Cantilever Beam Harvesting Model

Of the different techniques that can be employed to generate electricity across a piezo crystal, a cantilever beam structure is a commonly used method. The cantilever beam has one end fixed and another end free to move. A tip mass is attached on the free end. A thin piezo crystal film is sandwiched between two metal film plates an illustrated in Figure 5.5. In addition, this piezo-layer is imposed close to the fixed end in order to, creates more mechanical stress and higher electric current from the piezo layer. When the external vibration frequency matches the natural frequency of the beam, resonance occurs, which will cause the excessive deformation of the structure [49] and generate a higher electric dipole moment and potential difference in the piezo-crystal.
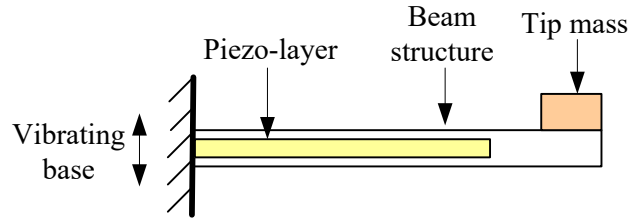
Figure 5.5. The schematic diagram of a cantilever beam structure for energy harvester.

The electrical voltage generated by a piezo crystal film due to vibration is a weak AC (alternating current) waveform signal, which is inadequate for general applications. To overcome this problem, an electric circuit is designed to amplify its magnitude and convert the AC signal to a DC (direct current) voltage signal. Figure 5.6 shows a diode rectifier circuit using a piezo-electric transducer (PZT), to rectify an AC to a DC voltage signal. A smoothing capacitor (C) is used to store the DC voltage charge, and to supply voltage to an external load.
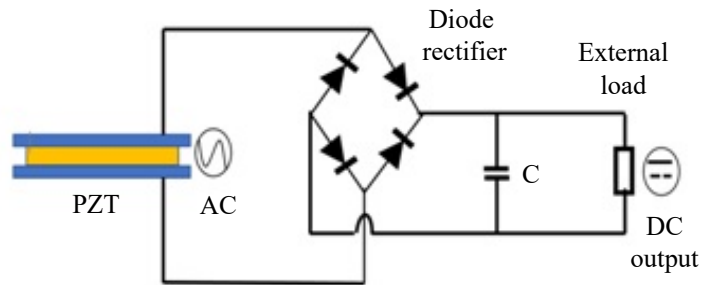
Figure 5.6. Basic schematic of an AC-DC system circuit.

5.3.1 System Parameters

In modeling a cantilever beam harvester, the related parameters include tip mass, equivalent beam stiffness, piezo-film length and thickness, and resonant frequency. The resonant frequency f_R can be computed by [50].

$$f_R = \frac{1}{2\pi}\sqrt{\frac{k}{m}} \qquad (5.1)$$

where k is the equivalent beam stiffness in N/m , and m is proof mass in kg.

The stiffness of the beam k is of marginal value. The proof mass includes structural mass. The resonant frequency depends on the beam structure and weight.

5.4 Some Issues in Designing Piezoelectric Energy Harvesters

A piezoelectric energy harvester is a resonance-based system. In order to generate the maximum power output, the beam should vibrate at its natural frequency or its harmonics. In applications, however, deviations from the resonance frequency will cause a decrease in vibration level and in turn, in power output [51]. The following presents a review of current solutions to scavenge more power at off-resonating frequencies.

5.4.1 Tuning Methods

Tuning the vibrational frequency is one of the prominent methods for generating power within a frequency range. A tuning setup serves as a damper to neutralize vibrations of the system [52], which can assist to excite higher vibration and scavenge more power output from the piezo-film. A few methods have been proposed in the literature for frequency tuning, which includes self-tuning and manual tuning modes [53, 54]. Self-tuning, as from the name implies, refers to as tuning that proceeds based on vibration properties automatically. Manual tuning, on the other hand, requires an external force to neutralize the vibration [55].

1) Magnetic Methods

Magnetic self-tuning uses an external resistive force to compensate vibration of energy harvester. Figure 5.7 shows the schematic structure of a typical magnetic harvester. It contains a pair of magnets, one of which is placed on the free end of the cantilever beam and another on the sliding part. The magnets are mounted on the system with opposite poles to generate attractive forces.

The magnet on the cantilever beam is subjected to attractive forces from an external tuned magnet. The vibration is neutralized by the related magnetic force. An adjustment slider is used to tune the location of the magnet to alter the stiffness value of a cantilever beam, as well as its resonant frequency (to be discussed in Equation 5.1). The distance between two magnets in this system is usually tuned manually. In addition, reliable clamping of the magnets on beam is difficult to achieve in a vibration environment. Losing clamping will lead to damage system failure.
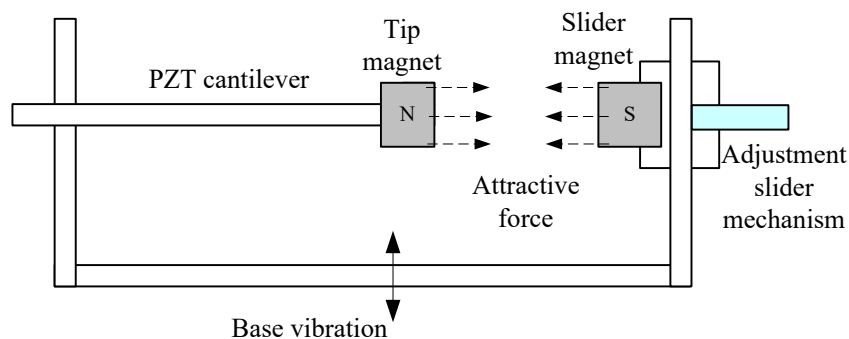
Figure 5.7. Schematic diagram of tunable harvester by magnets.

2) Rigid Stopper Method

As illustrated in Figure 5.8, a rigid stopper system consists of a PZT cantilever beam, a tip mass and a stopper. The stopper is used to restrict movement of the beam, or to limit the vibration amplitude. The stopper can also help to keep constant vibration amplitude so as to create the energy

harvester with a wider bandwidth. Properly locating the stopper position from the cantilever beam can control the bandwidth of the harvester [56].
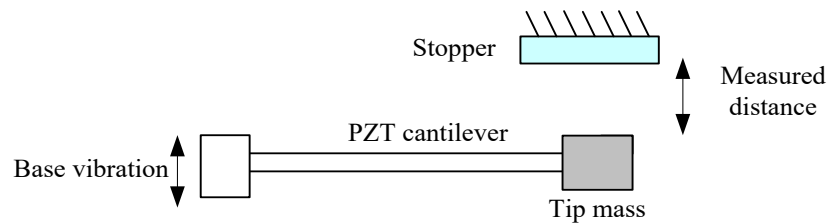
Figure 5.8. Schematic diagram of a rigid stopper.

The rigid stopper method is simple in structure, but it requires more space for fixing the stopper. The stiffness of vibrating cantilever beam changes abruptly from low to high value when the beam impacts the stopper.

5.4.2 Multimodal Energy Harvesting System

A multimodal energy harvesting system can match more than one frequency wideband excitation, by changing the size and shape of the piezo-energy harvester.

1) Spiral Shape Structure Energy Harvester

Figure 5.8 illustrates a multimodal energy harvester to increase the bandwidth of the resonance frequency with spiral-shaped energy harvester design [57]. It has eight metal plates fixed at the central point with a piezoelectric ceramic material. Each metal plate has a different length and will create a different resonance frequency when it is exposed to an excitation. Thus the harvesting system will demonstrate power output over a wider bandwidth range of frequency. However, this circular piezo-energy harvester is complex in structure, and is mainly used for high-frequency applications.
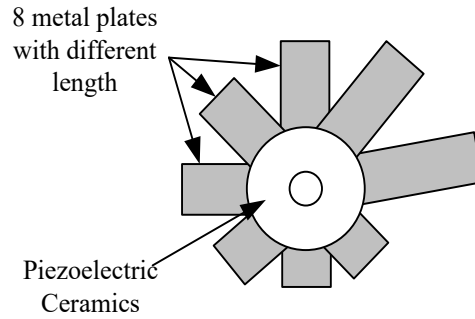
Figure 5.9. Schematic diagram of a spiral piezo energy harvester.

2) Multimodal Energy Harvester

Figure 5.10 shows a circular shape harvesting system for broadening frequency range [58]. It includes a high frequency generating beam (HFGB) with a PZT film, and multiple low-frequency driving beams (LFDB), each having a proof mass and a rope connected to the HFGB. The LFDB's are for low-frequency applications. If the vibration excitation is larger than the rope margin, it triggers the HFGB to oscillate. This harvester could achieve much wider bandwidth than traditional methods. But it is more complex in structure and requires more space to implement.
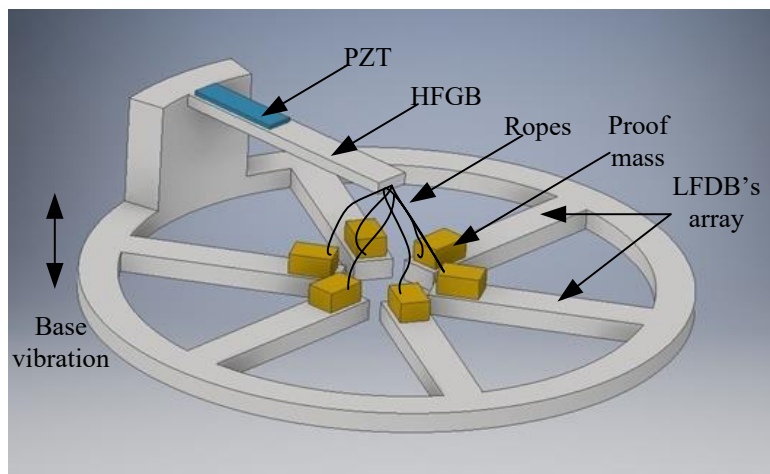
Figure 5.10. The architecture of a wideband vibration energy harvester: PZT: piezoelectric transducer, HFGB: high frequency generating beam, LFDB: low-frequency driving beam (retrieved from [58]).

Chapter 6 Development of the Piezoelectric Energy Harvesting System

6.1 Overview

An energy harvester generates electric energy and stores it for later use. Piezoelectric material is commonly used in the area of vibration-based energy harvesting systems, which has attracted a lot of R&D efforts in recent decade [49]. In principle, a piezoelectric energy harvester can use a conventional cantilever beam for vibration excitation as shown in Figure 6.1, where one end of the beam is fixed and other end is free. A tip mass is mounted at the free end of the beam to generate a vertical force due to vibration. A piezo-film layer is placed intermediate in the beam as is represented in Figure 6.1. During vibration excitation, the generated force on the beam F_y can activate the beam structure and initiate deformation/strain of the piezo-film in the corresponding direction.
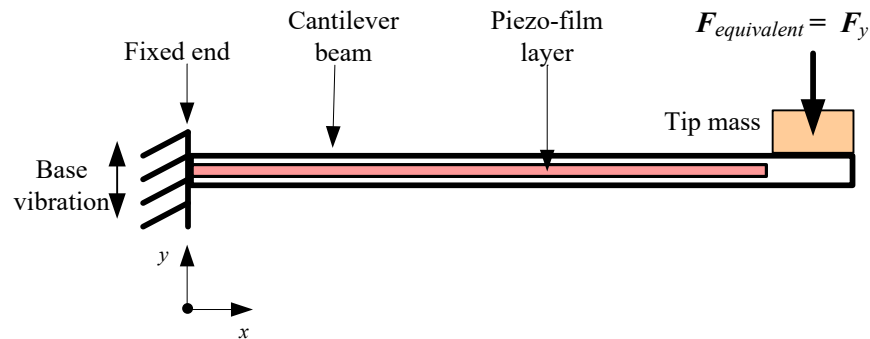
Figure 6.1. Force diagram of the conventional cantilever beam energy harvesting system.

The equivalent force $F_{equivalent}$ in the y-direction can be expressed as

$$F_{equivalent} = F_y = ma + mg \tag{6.1}$$

54

where m is the equivalent mass, g is gravitational acceleration, and a is the acceleration at that beam position.

6.2 The Proposed Energy Harvester

The schematic diagram of the proposed vibration energy harvester is shown in Figure 6.2. Different from the general cantilever beam harvester as illustrated in Figure 6.1, a specific support structure is added to the free end of the beam to generate an extra dynamic load to the beam.
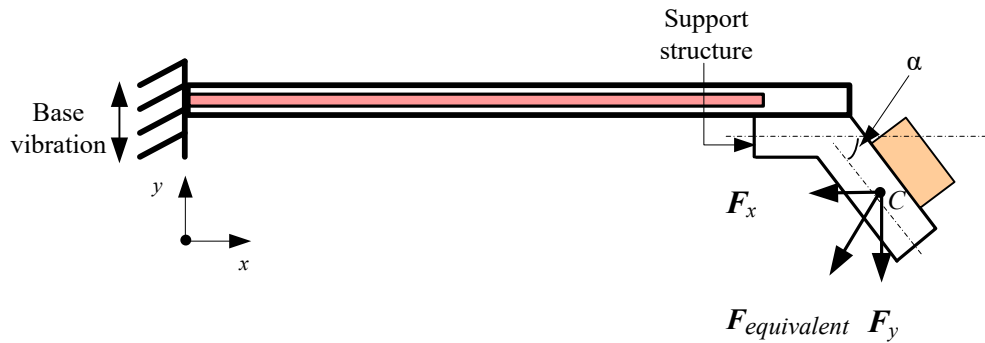
Figure 6.2. Force diagram of the proposed cantilever beam energy harvesting system.

Due to the angled acting force on the system, the equivalent force $\boldsymbol{F}_{equivalent}$ will be

$$\boldsymbol{F}_{equivalent} = \boldsymbol{F}_x + \boldsymbol{F}_y \qquad (6.2)$$

where $\boldsymbol{F}_x$ and $\boldsymbol{F}_y$ are the force components along the x-direction and the y-direction, respectively. The mass centroid of the tip mass is represented as C.

The vibration forces along the x- and y-direction enforce the piezo-film to deflect in the respective directions. In general, the more the piezo-film is deformed (or the higher the strain), the greater the amount of the power can be generated. The process of separating opposite charges within the piezoelectric material due to deformation is referred to as polarization. Polarization P

creates a voltage difference at the poles of the piezoelectric material for power generation. The polarization P and deformation d have the following relationship

$$P = d \times [J] \tag{6.3}$$

where d is the deformation (or mechanical strain); $[J]$ is the dielectric constant corresponding to specific piezoelectric material properties (e.g. for PZT 5H material, $[J]=3800$).

6.3 Beam Dynamics Analysis

6.3.1 Dynamic Load

The beam is subjected to variety of loading conditions. The load acting on a beam causes elastic deformation [59]. Consider a cantilever beam as shown in Figure 6.3(a). If F_y is the applied load, and L is length of cantilever beam, the deflection of beam at a distance x from fixed end is denoted as y_x can be represented as
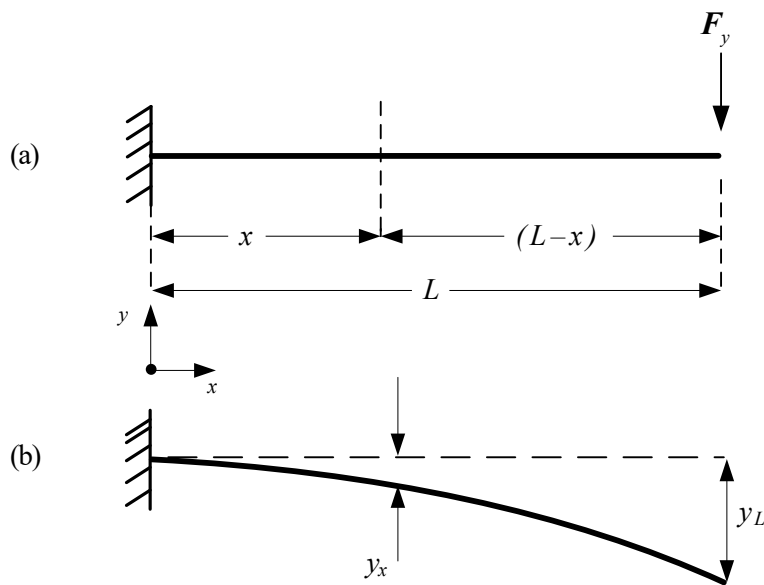
Figure 6.3. Bending of cantilever beam: (a) Beam with load, (b) Deflection curve

$$y_x = \frac{F_y\, x^2\, (3L - x)}{6EI} \tag{6.4}$$

where E is Young's modulus and I is moment of inertia of beam.

The deflection at free end will be

$$y_{x=L} = \frac{F_y L^3}{3EI} \tag{6.5}$$

Taking second derivative of Equation (6.4) with respect to x and rearranging terms, the acceleration can be expressed as

$$\ddot{y} = \frac{F_y}{EI}\, (L - x) \tag{6.6}$$

If m is the equivalent mass, the approximate equivalent dynamic load can be expressed as,

$$F_d = m\ddot{y} = \frac{m F_y}{EI}\, (L - x) \tag{6.7}$$

6.3.2 Dynamic Analysis

The dynamics analysis is to determine the internal loadings and the related deformation on the beam. In force analysis in two-dimensional condition, the internal forces and moment at a specific location of the beam can be determined through the free body diagram by the equilibrium conditions [59].

$$\Sigma\, \boldsymbol{F_x} = 0 \qquad\qquad \Sigma\, \boldsymbol{F_y} = 0 \qquad\qquad \Sigma\, \boldsymbol{M_O} = 0 \tag{6.8}$$

where $\boldsymbol{F_x}$ and $\boldsymbol{F_y}$ are the force components along the x-direction and the y-direction, respectively, and $\boldsymbol{M_O}$ is the moment about point O.

Consider a cantilever beam as shown in Figure 6.4(a). The F_y is applied equivalent vertical force on the free end (including both static and dynamic force components). To determine the internal loadings at cross-section A-A position x , using the method of sections, the free body diagram is shown Figure 6.4(b). Based on equations of equilibrium (6.8), the related internal loadings, normal force N_1, shear force V_1 and moment M_1 , can be determined
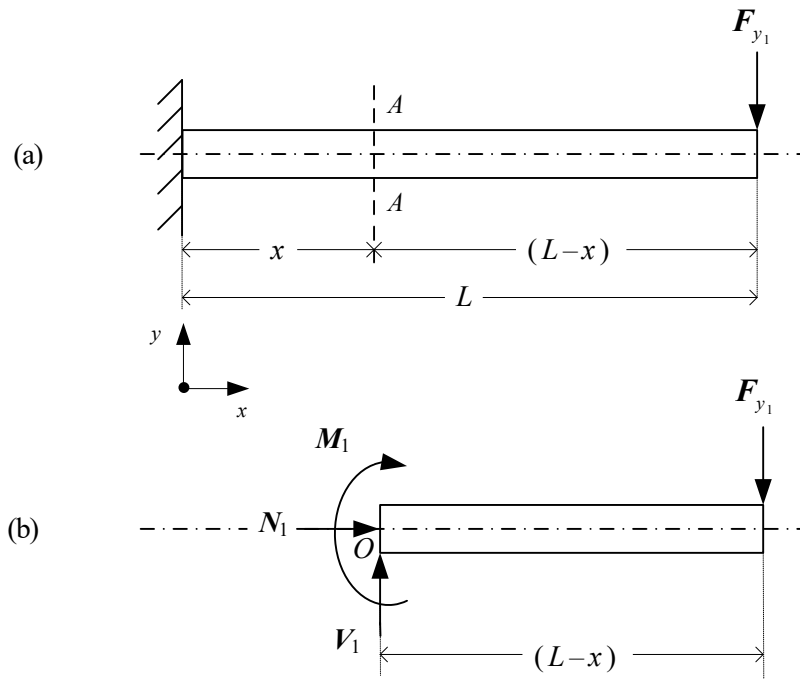
Figure 6.4. Cantilever beam with vertical applied force: (a) Force analysis of beam, (b) Free body diagram.

$$\Sigma F_x = N_1 = 0 \qquad\qquad N_1 = 0 \qquad\qquad (6.9)$$

$$\Sigma F_y = V_1 - F_{y_1} = 0 \qquad\qquad V_1 = F_{y_1} \qquad\qquad (6.10)$$

$$\Sigma M_O = F_{y_1}(L-x) + M_1 = 0 \qquad\qquad M_1 = -F_{y_1}(L-x) \qquad\qquad (6.11)$$

Similarly, force analysis is performed the proposed cantilever beam with an inclined support structure as shown in Figure 6.5(a). As a result of the support structure, the beam is

subjected to a dynamic force $\boldsymbol{F}_d$ as well as a static force mg. The corresponding force components along the x- and y-direction will be,

$$\boldsymbol{F}_{x_2} = \boldsymbol{F}_{dx} \tag{6.12}$$

$$\boldsymbol{F}_{y_2} = \boldsymbol{F}_{dy} + mg \tag{6.13}$$

Based on Equations of equilibrium (6.8) of the free body diagram in Figure 6.5(b), the internal loadings at section B-B can be determined by,
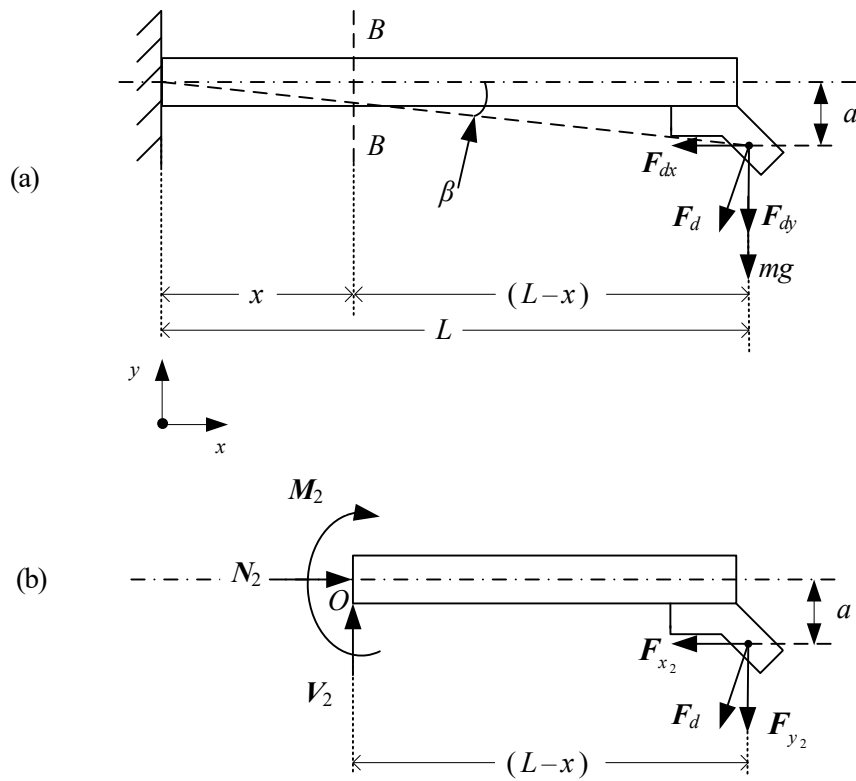
Figure 6.5. Cantilever beam with inclined applied force: (a) Force analysis of beam, (b) Free body diagram

$$\Sigma \boldsymbol{F}_x = N_2 - \boldsymbol{F}_{x_2} = 0 \qquad\qquad N_2 = \boldsymbol{F}_{x_2} \tag{6.14}$$

$$\Sigma \boldsymbol{F}_y = V_2 - \boldsymbol{F}_{y_2} = 0 \qquad\qquad V_2 = \boldsymbol{F}_{y_2} \tag{6.15}$$

$$\Sigma \boldsymbol{M}_O = \boldsymbol{F}_{y_2}(L-x) + \boldsymbol{F}_{x_2}(a) + M_2 = 0 \qquad\qquad M_2 = -\boldsymbol{F}_{y_2}(L-x) - \boldsymbol{F}_{x_2}(a) \tag{6.16}$$

With a comparison of Equations (6.11) and (6.16), the magnitude of the internal moment $| M_2 | > | M_1 |$. Correspondingly, the proposed beam with an inclined support structure will generate greater normal bending stress, and greater normal strain based on the Hooke's Law [59]. Correspondingly, more charges will be generated from the piezoelectric material. Similarly, comparing Equations (6.10) and (6.15), it is seen that $| V_2 | > | V_1 |$. More twisting shear stress will be generated in the proposed beam structure than a normal cantilever beam, which will result in more shear strain based on Hooke's law [59]. More charges will be generated from the piezo-film. From these investigations, the proposed beam with an inclined support structure will be more efficient to harvest piezoelectric energy, by enhancing polarization of the piezoelectric material to extract higher power at terminals.

6.4 Simulation Analysis

6.4.1 Beam Design Considerations

To verify the effectiveness of the proposed harvesting system, some simulation tests are undertaken prior to the fabrication of the related hardware. The simulation is performed using a commercial Autodesk Inventor software [60]. Autodesk Inventor can perform simulation analysis, and determine displacement, stresses, and strain effects resulting from different load conditions. Figure 6.6(a) shows the model of the proposed harvester. To make a comparison, the general cantilever beam with a normal load is simulated, whose model is shown in Figure 6.6(b).
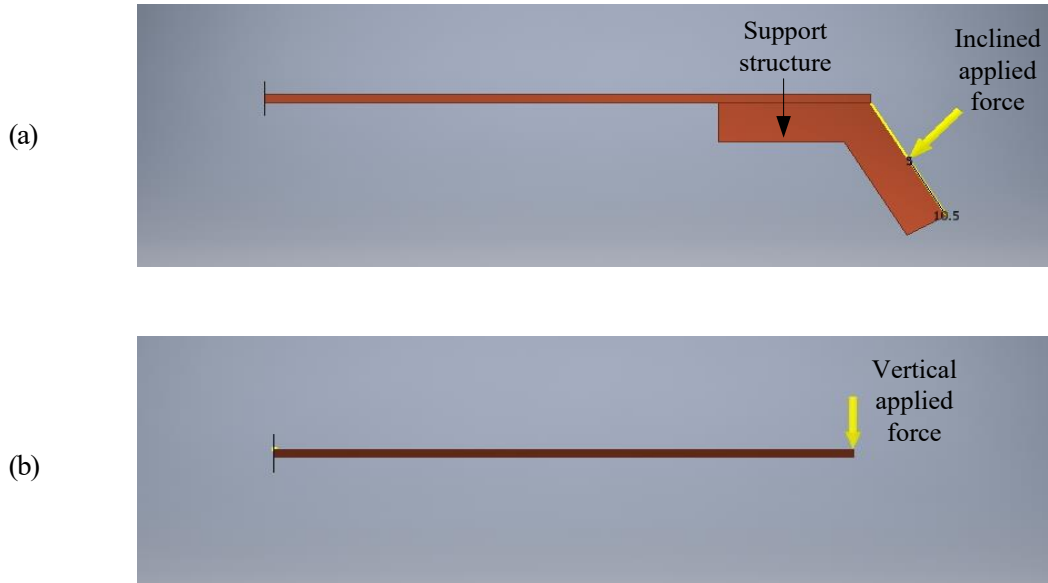
Figure 6.6. The simulation models: (a) Proposed cantilever beam, (b) Conventional cantilever beam.

To facilitate comparison, both beam models are assigned with the same materials as well as same geometrical dimensions. Copper is used for the beam materials. The piezo-film is Mide PPA-1014 and is sandwiched between copper materials. In order to treat system as cantilever beam, one side of beam is fixed and force is applied on other free end of beam as shown in Figure 6.6. The beam is formed through the use of finite element method in Autodesk inventor. 2D triangles are used with an aspect ratio of 1.5 and a maxiimum angle of 45degree. Both design and simulation of beam is utilized in inventor software. Table 6.1 summarizes the related parameters for these two models in this simulation test.

Table 6.1 Simulation test specification of design parameter for both models.

Parameter Name	Parameter Values
Length	40mm
Width	20.8mm
Thickness	0.71mm
Material	Copper
Mesh grading factor	1.5
Mass	20 gram
Applied force	0.196 N

6.4.2 Beam simulation

1) Deformation simulation

Taking into account of the simulation analysis, these two models are run to investigate the effects of the force components on the strain and displacement. Table 6.2 summarizes the force conditions in these simulation tests.

Table 6.2 Force analysis between conventional cantilever beam and proposed beam.

Conventional Cantilever Beam		Proposed Cantilever Beam	
Load Type	**Force**	**Load Type**	**Force**
Magnitude	0.196 N	Magnitude	0.196 N
Vector X	0.000 N	Vector X	-0.170 N
Vector Y	-0.196 N	Vector Y	-0.098 N
Vector Z	0.00 N	Vector Z	0.00 N

The equivalent strain represents a single mathematically equivalent strain from a three-dimensional strain state of beam[61], which provides a perception regarding the level of deformation occurred in the beam structure. Figure 6.7 and Figure 6.8 show the equivalent strain of the conventional cantilever beam and the proposed harvester model. If deformation of beam is measured as the bending deflection from its original position, the related results are summarized in Table 6.3. It can seen that compared to a conventional cantilever beam (3.521×10^{-5}), the proposed harvester design can generate higher strain (1.579×10^{-4}) along the beam.
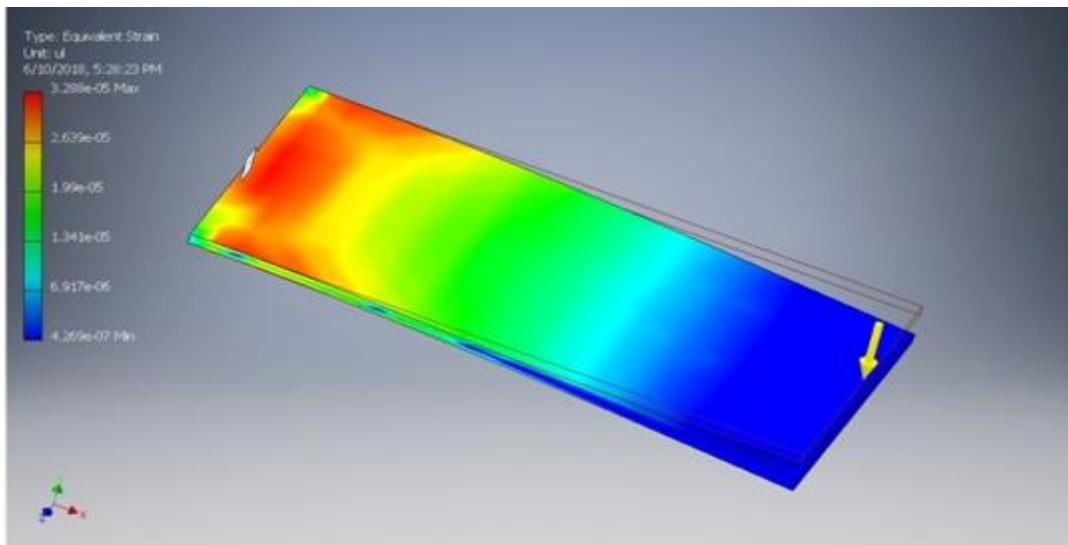
Figure 6.7. Equivalent strain of a conventional cantilever beam.
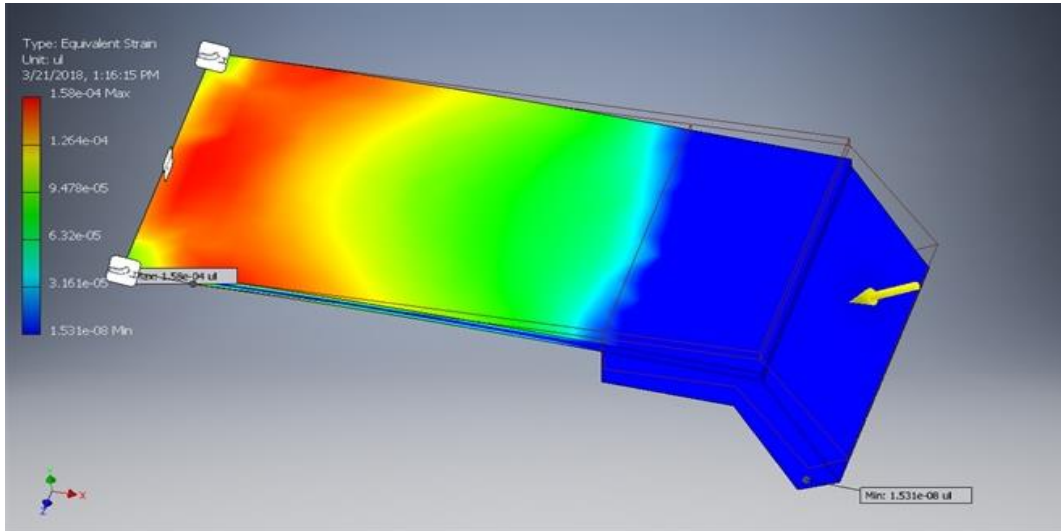
Figure 6.8. Equivalent strain of the proposed cantilever.

Table 6.3. Summary of the simulation resultswea

Conventional Cantilever Beam		Proposed Cantilever Beam	
Parameters	**Value**	**Parameter**	**Value**
Deformation	0.091 mm	Deformation	0.356 mm
Maximum equivalent Strain	3.521×10^{-5}	Maximum equivalent Strain	1.579×10^{-4}

It is seen from simulation that the equivalent strain and deformation of the proposed harvester is much higher than that of the conventional cantilever beam. It deforms along both the vertical and longitudinal directions. Correspondingly, more comprehensive deformation/strain is generated in the beam, and more power will be generated in the harvester. Additionaly, simulation results showed proposed beam undergoes large stress (4.461 MPa) than simple conatilever beam (1.705 MPa). Therefore, the proposed cantilever harvester is more efficient in energy harvesting than a general cantilever harvester.

2) Optimal angle simulation

Next, simulation analysis will be undertaken to examine the effects of supporter angle on the energy harvester. Three simulations are performed with supporter angles of $\alpha = 30°$, $45°$, $60°$, $65°$, $90°$. The corresponding simulation results are shown in Figure 6.9. The related results are summarized in Table 6.4.

(a)

(b)

(c)

(d)

(e)
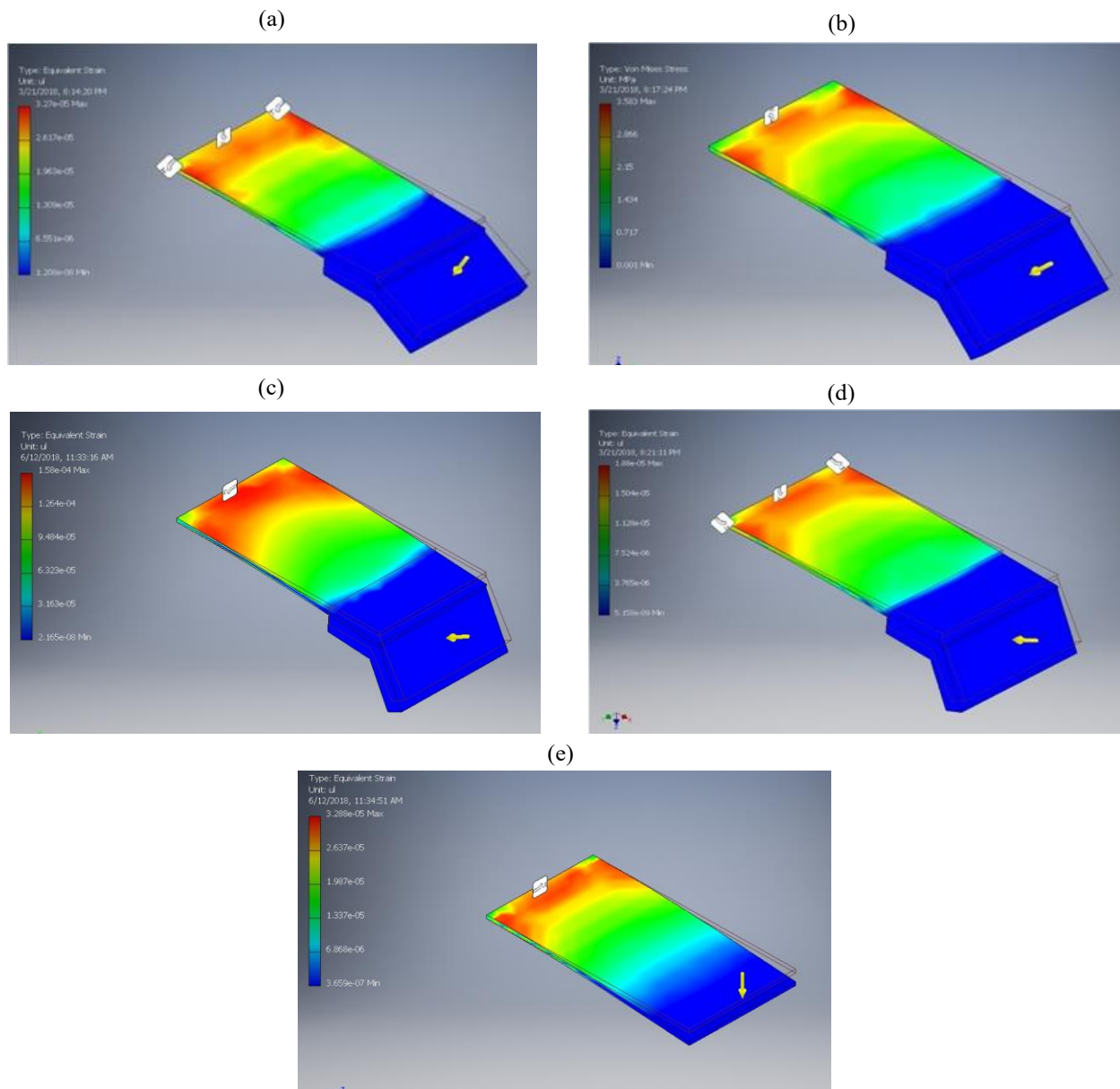
Figure 6.9. Equivalent strain simulation corresponding to different values of α angle support structure: (a) 30°, (b) 45°, (c) 60°, (d) 65° (e) 90°

Table 6.4. Simulation analysis of different angle results.

Parameters	Angle (α)				
	30°	45°	60°	65°	90°
Deformation (mm)	0.123	0.215	0.356	0.249	0.091
Maximum equivalent Strain	8.789×10^{-5}	0.145×10^{-4}	1.579×10^{-4}	0.985×10^{-5}	3.521×10^{-5}

From the related equivalent strain distributions in Figure 6.7 corresponding to angles of 30°, 45°, 65°, 90° as well as the test results from Table 6.4, that the maximum strain is generated when $\alpha = 60°$. From Table 6.4, it is seen that supporter structure with $\alpha = 60°$ is the optimal inclination angle in this case.

6.5 The Developed Energy Harvesting System

According to simulation investigation of the theoretical model proposed in subsection 6.4.2, a prototype is developed for testing, as shown in Figure 6.10.

(a)   (b)
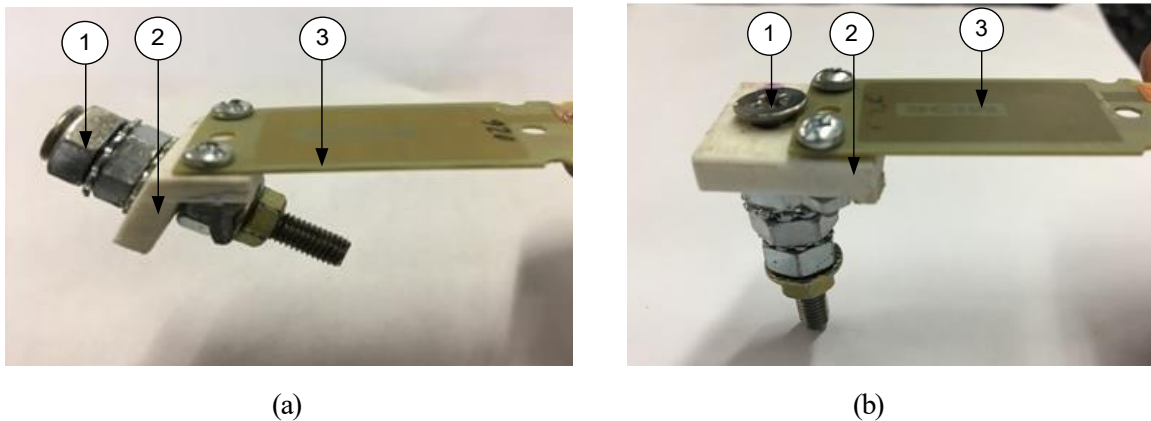
Figure 6.10. Prototype models: (a) With an angular supporter, (b) With a straight supporter: (1) Proof mass, (2) Support structure, (3) Piezo-transducer.

The developed energy harvester consists of a piezoelectric transducer (or PZT), a proof mass, and a support structure. The PZT a single layer piezo-film PPA-1014, which is made from MIDE [62]. This PZT has properties like effective stiffness, smaller dimension (53 mm× 20.8 mm), and high natural frequency (506 Hz). It exhibits ideal performance especially at low resonating frequency.

The proof mass is the combination of several small pieces of washers and nuts to facilitate changing of the applied load. Based on the theoretical model analysis, the proof mass is 20 grams in this case. The proof mass is clamped to the free end of the transducer by using a pair of bolts.

The supporter is made using a 3D printer. The supporter is designed with five inclination angles $\alpha =$ 30°, 45°, 60° 65°, 90° where $\alpha = 60°$ is the optimal angle in this case, based on simulation analysis in section 6.4.2.

6.6 Power Charging System

The purpose of the developed energy harvester is to convert vibration energy to electric power so as to charge the related batteries in the smart temperature sensors. Figure 6.11 illustrates a simplified circuit for this charging system. The main chip is LTC-3588, which is used to amplify the signal, perform wave rectification, and convert the generated AC signal to a DC signal to charge batteries or capacitors.
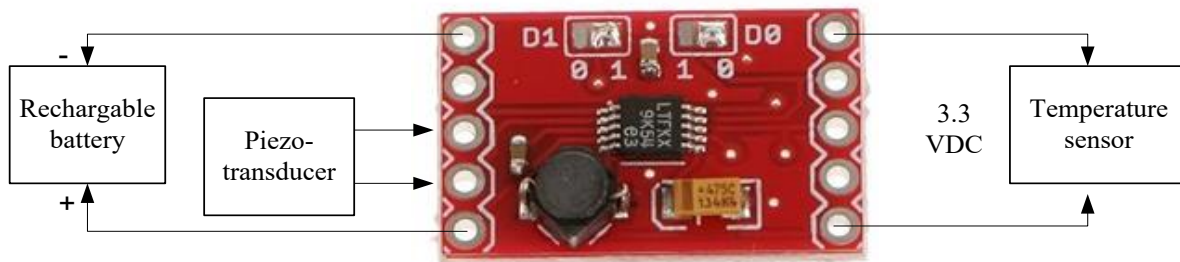
Figure 6.11. A simplified circuitry of LTC 3588-based piezoelectric energy harvester.

6.7 Performance Evaluation of the Developed Energy Harvester

6.7.1 Experimental Setup

The effectiveness of the developed energy harvester is tested, using an established experimental setup as shown in Figure 6.12. The experimental setup consists of a vibration shaker, a test bed, a signal generator, a power amplifier, an oscilloscope, a piezoelectric transducer prototype, LTC-3588 circuit board and a rechargeable battery set.
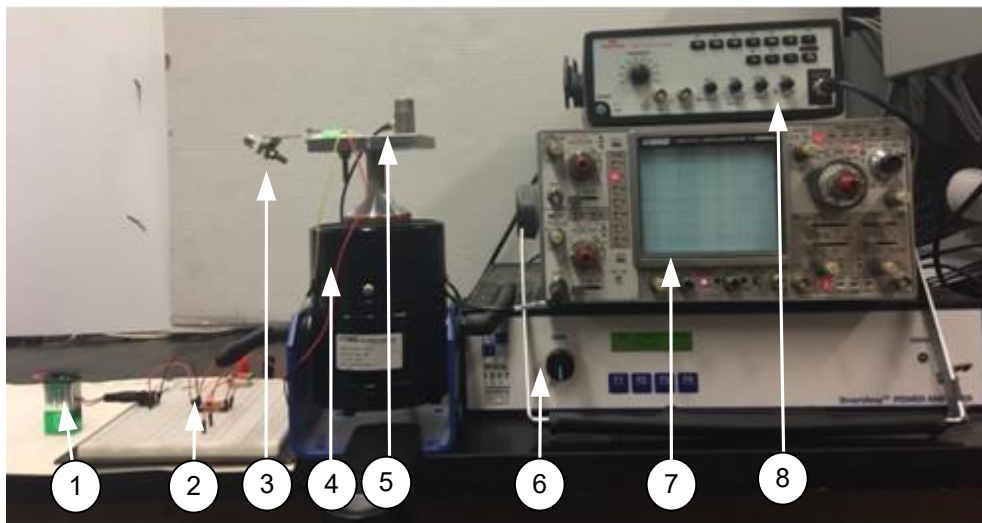
Figure 6.12. Piezoelectric energy harvester experimental setup: 1) Battery, 2) LTC-3588 circuit board, 3) Piezo-transducer prototype, 4) Shaker equipment, (5) Shaker testing bed, 6) Power amplifier, 7) Oscilloscope, 8) Signal generator.

A shaker is used to excite vibration of the tested structure or frame. The shaker used in this work is a TMS 2025E device, which has wide frequency range and amplitude adjustment configurations. The tested harvester is installed to the test bed of the shaker.

The signal generator (FG2C from Meterman) is an equipment to provide the related signals to the shaker. It can generate signals in different forms such as sinusoidal, square. The sinusoidal signal is followed in testing.

The power amplifier (2100E21 from Modal Shop Inc.) is used to amplifying the signal amplitude from the signal generator cannot, so as to excite the shaker.

An accelerometer (PCB 301A12 ICP) is used to measure vibration and g-force in the test bed. The sensor sensitivity is 0.480mV/g.

An oscilloscope (1590A from BK precision) is used to observe the properties of electrical signal over time and monitor the electric voltage output generated from the energy harvester. The related results will be analyzed in a computer by the use of an interface hardware developed for this test.

6.7.2 Performance Evaluation of the Developed Energy Harvester

1) Tested Vibration Energy Harvesters

A series of tests have been performed using the stated experimental setup. Figure 6.13 shows the tested harvesters. The purpose is to examine the effectiveness of the developed energy harvesting system in terms of charge generation and power saving.

(a)   (b)
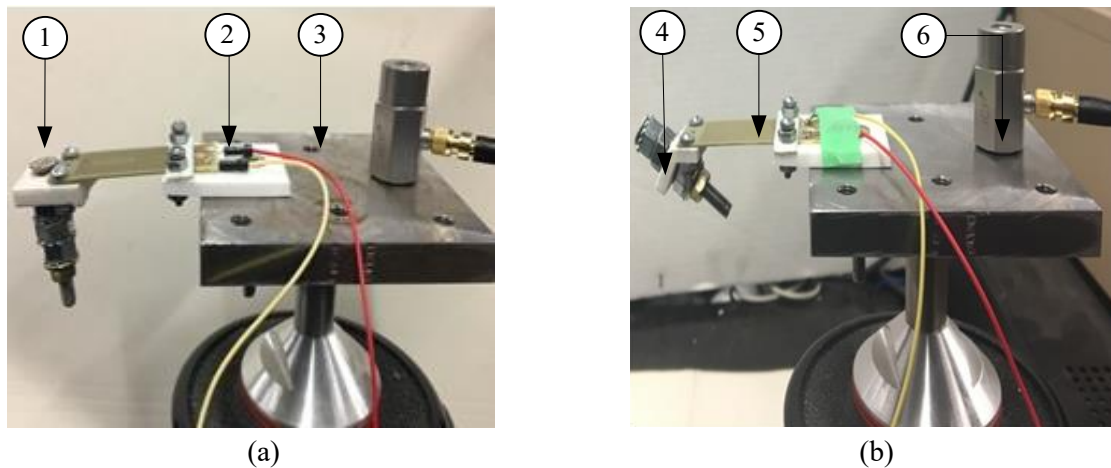
Figure 6.13. Two experimental setups in testing: (a) A conventional cantilever beam, (b) The proposed cantilever beam: (1) The tip mass, (2) Piezoelectric electrical terminal, (3) Testing bed , (4) The supporter, (5) The piezo transducer, (6) The accelerometer.

2) Power Generation:

This section presents experimental results related to power generation. From initial testing, resonant frequency is found to be around 22Hz with respect to 20-grams of tip mass on the harvesting system. The tests are executed with a varying frequency between 10 Hz and 30 Hz, which also covers the range of vibration frequency of general truck vehicles [63]. The vibration amplitude value is fixed at acceleration of about 0.5g for both beams over the tested frequency range.

Figure 6.14 shows the voltage response results recorded with the potential difference measured across LTC-3588 output poles, with open circuit or without the connection to the charger. It is seen that the voltage response shows a peak at the resonant frequency of 22 Hz for the traditional beam harvester. But even a slight variation in frequency can cause a significant reduction in energy output. On the other hand, proposed harvester shows high voltage between 19 to 24 Hz frequencies due to its efficient supporter structure.
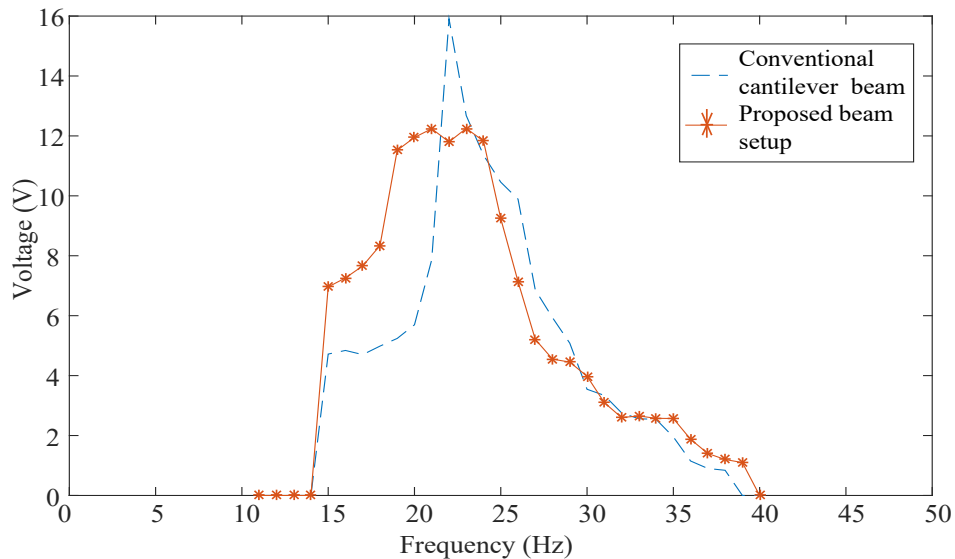
Figure 6.14. Comparison of voltage output from the proposed harvester and the conventional beam.

Figure 6.15 illustrates the comparison of current responses from the developed energy harvester and the conventional cantilever beam. It is clear that the proposed harvester has a wider current response bandwidth than that of the conventional beam setup. The current response at the resonance frequency is observed about 0.25mA. The proposed harvester shows more robust in applications.
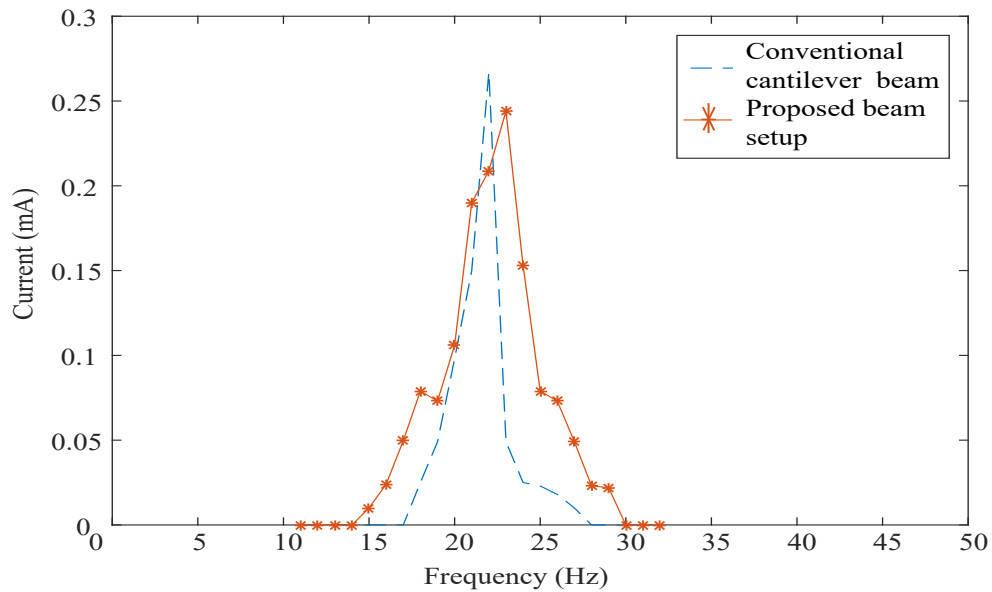
Figure 6.15. Comparison of current response curve to the proposed beam and conventional beam.

Figure 6.16 illustrates the overall power response (i.e., product of voltage and current) of these two energy harvesters. Although the maximum power value 2.9 mW from the proposed energy harvester is lower than that generated by the conventional cantilever beam (about 4.3 mW), the power response configuration of the proposed harvester is much wider in bandwidth and robust in power generation. In addition, 2.9 mW is high enough for our required battery charging purposes.
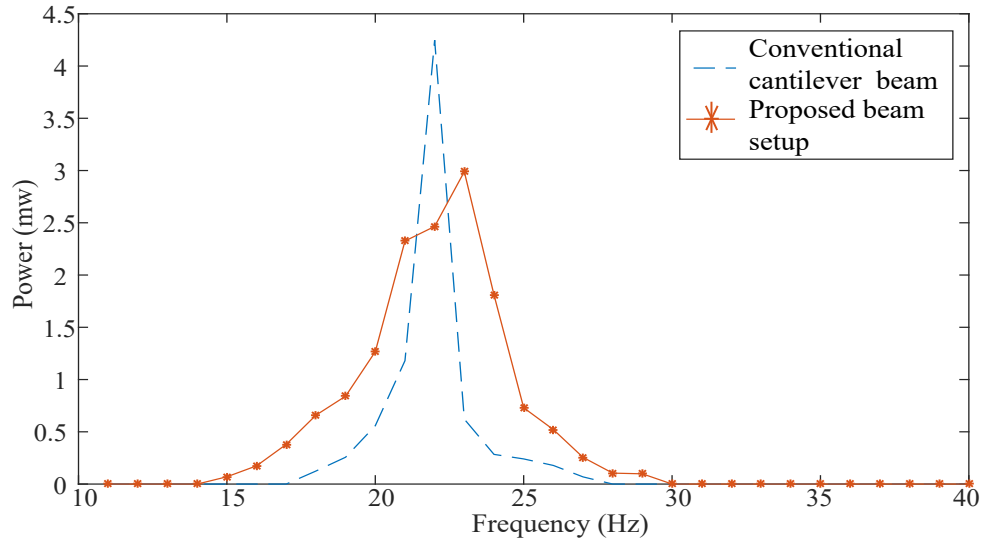
Figure 6.16. Comparison of power response curve to the proposed beam and conventional beam.

3) Battery Charging

Above tests are related to open circuit conditions without loading (i.e., not charging batteries). The testing of battery charging capability is discussed in this subsection. Energy harvesters are tested over 30 min to charge the battery (longer time running will result in overheating of the shaker equipment). Firstly, the shaker is running at the resonant frequency of 22 Hz. The battery is placed in a hard glass bottle for safety purpose. It is seen that the developed energy harvester can charge the battery from 0.79V to 1.18V over 30 min, with an increase of 0.39V. Similarly some tests are performed at different off-resonant frequencies to replicate condition of vibrations on vehicle. Table 6.5 summarizes some battery charging test results using the proposed energy harvester over a few frequencies.

Table 6.5. Observation of battery charging status over 30 min test run.

Conditions (Hz)	Voltage Increment (V)
22	0.39
21	0.24
20	0.25
18	0.22

Chapter 7 Conclusion

7.1 Conclusions

Brake system reliability is critical to safe driving of vehicles. In operation, a brake converts the kinetic and potential energy of the vehicle into heat energy. If heat is not dissipated properly, for example, when a truck is going downhill and the brakes are continuously operated, brake components are subjected to overheating, which will deteriorate braking functions and can cause serious safety problems. The objective of this research is to investigate different cooling solutions and develop a new intelligent air cooling system for drum brake cooling in trucks.

Several experimental setups have been developed to test different cooling solutions, such as a blower-based air cooling, a water cooling, and an air compressor-based air cooling. Findings have confirmed that the blower system cannot provide sufficient flow rate to cool the brake drums. Although water cooling is effective to dissipate heat, it may not be an optimal solution especially in winter season, as water will freeze in the tank. In addition, the discharged water could pollute the street.

This work will focus on compressed air cooling. A specific air compressor (designed by our research team) will be used to high flow rate but low-pressure air source for this cooling system. An automatic controller is designed to control the performance of the cooling system based on the information from drum temperature. To provide sufficient power source to the temperature sensors, a piezoelectric energy harvester has been developed to convert ambient vibrations to electrical voltage. A new energy harvesting transducer is proposed to improve power generation efficiency. The test results have shown that the developed energy harvester can generate between

0.65mW to 2.9mW over the common truck operation bandwidth of 18Hz to 25Hz. Test results show that the harvester can meet the battery charging requirements of this project.

7.2 Contribution of This Study

The following summarizes the related contributions made through the course of this study:

- Three experimental setups have been developed and the related tests have been performed with water cooling, blow-air cooling, and compressed air cooling system to investigate the brake drum cooling principles and characteristics.

- A new intelligent cooling system has been designed for truck drum braking cooling. The designed air compressors can provide air sources to meet our specific requirements such as higher air flow rate, low pressure, and ease of automatic control implementation.

- A vibration energy harvester has been developed to convert vibration energy from the truck axis to electrical energy to charge batteries in smart temperature sensors.

- The harvester structure is optimized in terms of supporter angle to provide best energy converting efficiency.

7.3 Future Work

Current R&D work is at the level of prototypes at lab environment. The following summarizes the future work related to this thesis project:

- Current design and testing of the air cooling system focuses on one wheel only. The system will be implemented to multiple wheels in a truck for real-time application.

- Test and improve the developed piezoelectric energy harvester to cover variable vibration frequency conditions.

References

[1]   Fred Puhn, "Disc & drum brake," in *Brake handbook*, HP trade, 1987, p. 176.

[2]   S. Baseley, C. Ehret, E. Greif, M. g. Kliffken, "Hydraulic hybrid systems for commercial vehicles," in *Commercial Vehicle Engineering Congress & Exhibition*, 2007.

[3]   S. habla, "THE EICHHOLZ," 2011. [Online]. Available: 2018. [Accessed 2nd April 2018].

[4]   T. M. Haynes, "Disc brakes," in *Automotive Disc brake Manual: The complete*, Haynes, 1999, p. 128.

[5]   Toyota, "Drum Brakes-section 3," in *Toyota Brake Systems- Course 552*, 2010.

[6]   J. D. Halderman, , Automotive Brake Systems, Pearson, 1995.

[7]   A. I. 102, "COMSOL," 2012. [Online]. Available: https://cdn.comsol.com/wordpress/2013 /02/Step-by-step-guide-for-modeling-heat-generation - in-a - disc - brake.pdf. [Accessed 5 Ma rch 2017].

[8]   A. L. A. Costa, M. Natalini, M. F. Inglese, O. A. M Xavier, "Tire Bead Overheating in Urban Buses and Trucks Using Drum Brake System," *Tire Science and Technology,* vol. 26, no. 1, pp. 51-62, 1998.

[9]   R. bilfjadraar, "ranas bilfjadraar/bake fade," [Online]. Available: https://ranasbilfjadrar.wo rdpress.com/2016/03/29/brake-fade/. [Accessed 15 january 2108].

[10] Z. Zhu, J. Bao, Y. Yin and G. Chen, "Frictional catastrophe behavior and Mechanisms of brake shoe for mine hoist during repetitious emergency braking," *Industrial Lubrication and tribology,* vol. 65, no. 4, p. 6, 2013.

[11] S. News, "Semitrailer fire slows traffic on Bluff street," STGnews, St. George, 2016.

[12] K. Ashok, "Thermal analysis of Brake drum," 2017. [Online].

[13] J. R. Barber, "The influence of thermal expansion on the friction and wear process," *Wear,* vol. 10, no. 2, pp. 155-159, 1967.

[14] D. Cottingham, "Overheating brakes and brake fade," [Online]. Available: https://mocktheorytest.com/resources/overheating-brakes-and-brake-fade-what-can-you-do/. [Accessed 12 January 2018].

[15] 王佳琦, 刘志龙, 刘向阳 and 白弘基 , "An automotive brake overheating failure active intervention system and control method". China Patent CN 104908735B, 22 08 2017.

[16] R.-t. ramps, "car and driver," feature, 7 October 2010 . [Online]. Available: https://www.caranddriver.com/features/runaway-truck-ramps-explained-feature. [Accessed 1 january 2018].

[17] R. Sunil and S. R. Shankar, "Design and Development of Bimetal Brake Drum to Improve Heat Dissipation and Weight Reduction.," *SAE Technical Paper series,* 2014.

[18] W. Fitzpatrick, "Water-cooled brake drum". Patent US 2098490 A, 1937.

[19] R. Bloss, "Water cooled brake". Patent US 2299208, 1942.

[20] 靳增鑫李学峰徐大伟, "Brake drum water-spraying method, auxiliary system and vehicle". Patent CN 103057530 A, 2013.

[21] C. Tata Motors, "Tatamotors," 2018. [Online]. Available: http://www.tatamotors.com.my/press/tata-motors-becomes-futuready-with-the-all-new-powerful-1000-bhp-prima-race-truck/. [Accessed 1st June 2018].

[22] L. TROY, "brake cooling system". Patent US 3347344, 1967.

[23] A. B. a. team.Patent US 8678426 B1, 2014.

[24] S. A. N. a. team, "Brake cooling system". Patent US 6315091, 2001.

[25] B. D. H. a. team.Patent US 2003/0047394 A1, 2003.

[26] B. Shome, V. Kumar, S. Chacko, V. Paluskar and M. Shridhare, "Numerical Simulation of Drum Brake Cooling for Heavy Trucks," 2006.

[27] M. G. Scott, "Water and air cooled brake drum". Patent US 2982378, 1961.

[28] J. Ellingson, S. Davie and Z. Mazurek, "Design of an Active Brake Cooling System," Lakehead University, Thunder Bay, 2017.

[29] B. o. E. efficiency, "Chapter 3 Compressed Air system," [Online]. Available: http://www.e m-ea.org/guide%20books/book-3/chapter%203.3 % 20 compressed%20air%20system.pdf. [Accessed 22 11 2017].

[30] C. Technologies, "Air compressor types and controls," in *CEA technologies refernce guidebook*, Ontario, CEATI, 2007, p. 118.

[31] Blackmer, "Gas equipments/ catalogs/blackmer," 04 1999. [Online]. Available: http://www.gasequipment.com/catalogs/cryogenic/pdf/Blackmer/Compressors/Comp%20 Selection%20and%20Sizing.pdf. [Accessed 2017 05 15].

[32] J. Klly, "4 Benefits of installing a two-stage air compressor," [Online]. Available: https://www.jerrykelly.com/blog/2012/june/4-benefits-of-installing-a-two-stage-air-compres/. [Accessed 25 05 2017].

[33] C. A. &. G. Institute, "Selection of air compressor," in *CAGI handbook*, Cleveland,Ohio, Thomas Associates, Inc., 2016, p. 29.

[34] C. E. Calc, "Vcommons/stroke length by Kurt Heckman," 2017. [Online]. Available: https://www.vcalc.com/wiki/KurtHeckman/stroke+length. [Accessed 27 05 2017].

[35] B. Malcolm, "Electrical enginerring portal/ Electrical and Mechanical losses," Practical Variable Spped Drives, 07 2014. [Online]. Available: https://electrical-engineering-portal.com/cooling-and-ventilation-of-electric-motors-ic. [Accessed 02 06 2017].

[36] P. Luong, "The Development of Intelligent Control System," Lab for Intelligent Mechatronics System , Lakehead University, Thunder Bay, 207.

[37] K. M. Passno, "The overview of Technique," in *Intelligent Control*, Columbus, 2015, p. 34.

[38] Spark fun, "Spark fun product," MLX90614, [Online]. Available: https://www.sparkfun.com/products/9570.

[39] Atmel, "ATmega328/P Datasheet summary," ATmel, 2016.

[40] Resistorguide, "Pull up resistor/ pull down resistor," 2016.

[41] P. Wang and R. Gray, "A wireless Temperature sensor Powered by piezoelectric Energy Harvesting System," *IEEE,* vol. 15, no. 2, p. 4, 2015.

[42] A. Blakers, "THE CONVERSATION," 25 March 2013. [Online]. Available: http://theconversation.com/explainer-what-is-photovoltaic-solar-energy-12924. [Accessed 2018 12 May].

[43] Energy Efficiency & Renewable Energy, "Advantages and Challenges of Wind Energy," 2015. [Online]. Available: https://www.energy.gov/eere/wind/advantages-and-challenges-wind-energy. [Accessed 24 April 2018].

[44] R. L. Harne, K. W. Wang, "A review of the recent research on vibration energy harvesting via bistable systems," *IOP Publishing Ltd,* vol. 22, no. 2, 2013.

[45] C. A. Howells, "Piezoelectric energy harvesting," *Energy Conversion and Management,* vol. 50, no. 7, pp. 1847-1850, 2009.

[46] P. Dineva and et. al., Dynamic fracture of Piezoelectric Materials, Switzerland: Springer Internationa, 2014.

[47] Wikipedia, "Piezoelectricity," [Online]. Available: https://en.wikipedia.org/wiki/Piezoelectricity. [Accessed 12 12 2017].

[48] S. datta, "Piezoelectric Materials: Crystal Orientation and Poling Direction," Comsol Blog, 14 February 2014. [Online]. Available: https://www.comsol.com/blogs/piezoelectric-materials-crystal-orientation-poling-direction/. [Accessed 3 February 2018].

[49] D. Motter, J. V. Lavarda and S. Silva, "Vibration energy harvesting using piezoelectric transducer and non-controlled rectifiers circuits," *Journal* .

[50] Manish and Sukesha, "Piezoelectric energy harvesting in wireless sensor networks," *International Conference on Recent Advances,* 2015.

[51] D. H. Zervos, "Piezoelectric energy harvesting: Developments, challenges, future," *Research article (IDTechEx),* 10 January 2013.

[52] S. Herold and D. Mayer, "Adaptive Piezoelectric Absorber for Active Vibration Control," *MPDI journal/ actuators,* vol. 5, no. 7, p. 13, 2016.

[53] P. E. E. Wellstead, M. B. Zarrop, Self-tuning systems: control and signal processing, New York: John Wiley & Sons Inc., 1991.

[54] M. Lallart, S. R. Anton, D. J. Inman, "Frequency self-tuning scheme for broadband vibration energy harvesting," *Intelligent Material Systems and Structures,* vol. 21, no. 9, pp. 897-907, 2010.

[55] K. S. Jin Tam, "Automated tuning of a piezoelectric power harvesting cantilever beam via the application of an axial load," Ryerson University, Toronto, 2013.

[56] L. Dhakar, H. Liu, F. Tay and C. Lee, "A new energy harvester design for high power output at low frequencies," *Sensors and Actuators A: Physical,* p. 9, 2013.

[57] H. Gulec, A. G. Akyurekli, M. Gul, M. Gurbuz, B. Koc and A. Dogan, "Wide-Band Piezoelectric Resonance Frequency Energy Harvester," *IEEE,* p. 4, 2014.

[58] J. Zhang, L. Kong, L. Zhang, F. li, W. Zhou, S. Ma and L. Qin, "A Novel Ropes-Driven Wideband Piezoelectric Vibration Energy Harvester," *Applied Sciences,* vol. 12, p. 6, 2016.

[59] J. Gere and B. Goodno, Mechanics of Materials, Stamford: Cengage Learning, 2013.

[60] "Anylogic," anylogic simulations, [Online]. Available: https://www.anylogic.com/use-of-simulation/. [Accessed 27 Feb 2018].

[61] Autodesk, "Autodesk knowledge network," Autodesk, [Online]. Available: https://knowle dge.autodesk.com/support/inventor-products/learn-explore/caas/CloudHelp/cloudhelp/201

4/ENU/Inventor/files/GUID-C787792D-BBB1-41A7-BBD7-CBCABCBE7C01-htm.html. [Accessed 12 03 2018].

[62] M. technology, "PPA products Mide technology," [Online]. Available: https://www.mouser.com/ds/2/606/ppa-piezo-product-datasheet-844547.pdf. [Accessed 9 9 2017].

[63] M. T. Trailer, "Determine Wheel speed or Vibration using Smart phone and frequency measurement," International delivers, Thunder Bay, 2017.

[64] BAT-Auto, "P0500- Vehicle speed sensor-circuit information," 2017. [Online]. Available: https://www.troublecodes.net/pcodes/p0500/.

Appendix

Measurement of Vehicle Speed Sensor Magnitude

The vehicle speed sensor is typically mounted on differential or transmission assembly of the vehicle. The speed sensor provides speed information to the electronic control unit of the vehicle. This information is used for various function in vehicle (e.g., speedometer operation). Permanent magnet sensor is mostly used in vehicle [64]. This type of sensor creates an AC voltage signal that is proportional to vehicle speed as shown in figure A.1(a). The sensor rotor with rectangular teeth on curvature is bolted to vehicle driveline rotor shaft. Sensor creates a magnetic field. When a teeth part of the rotor passes through the sensor magnetic field, AC voltage signal is created. Higher speed shows high voltage magnitude and lower speed shoes low magnitude in information. The position of the vehicle speed sensor on the truck is represented in Figure A.1(b).

At the beginning of intelligent control system development, vehicle speed information was taken into consideration to switching motor to turn on and off. The vehicle speed decreases due to the application of brakes. Then vehicle sensor sends lower magnitude of the voltage signal to electronic con control circuit. The objective behind this investigation was to provide this reading of low magnitude signal information to turn on cooling air compressor switch by use of control system.
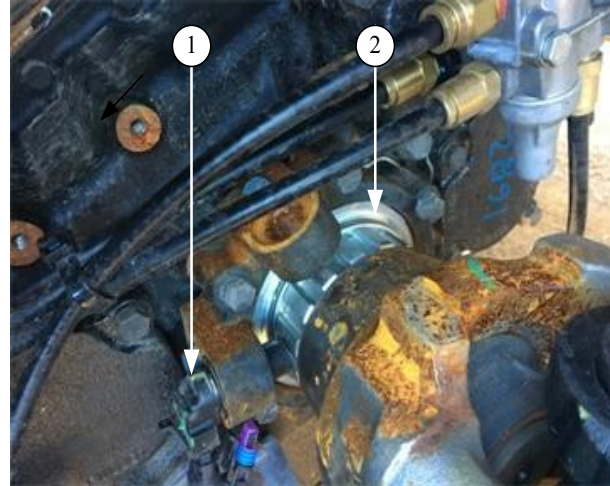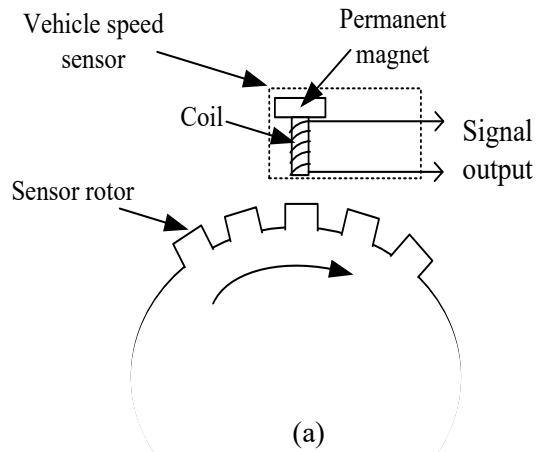
Figure A.1. Vehicle speed sensor: (a) Schematic of permanent magnet speed sensor, (b) mounting location of speed sensor on the truck: (1) Vehicle speed sensor, (2) Sensor rotor.

The testing has been performed in Maxim Truck and Trailer Pvt. Ltd. Company to analyze the behavior of change in magnitude at various speed levels. The rear axle of the truck (model LT 625 6X4 from International Ltd.) is towed by use of an industrial towing vehicle as shown in Figure A.2. An oscilloscope is connected to read voltage magnitude of the sensor.

From some initial testing, some conclusions can be obtained.

1) Test results show that the sudden change in magnitude of voltage occurs with the difference in vehicle speed.

2) Fluctuation of voltage magnitude would create an interrupt problem in microcontroller unit. This could cause to halting issue during working of the cooling system.

3) The permanent magnet speed sensors are sensitive and magnetic flux from their surroundings (e.g. wires) can render results inaccurate [64].

Due to these limitations, the proposed intelligent control system considered a temperature measuring sensor for switching the air compressor motor.

Figure A.2. Speed sensor testing investigation performed in Maxim Truck & Trailer company: (1)Transportation truck, (2) Rear axle towed, (3) Industrial towing vehicle.